OPTOFLUIDIC REACTORS FOR SUSTAINABILITY AND ENERGY APPLICATIONS

A Dissertation

Presented to the Faculty of the Graduate School

of Cornell University

in Partial Fulfillment of the Requirements for the Degree of

Doctor of Philosophy

by

Syed Saad Ahsan

January 2015

OPTOFLUIDIC REACTORS FOR SUSTAINABILITY AND ENERGY APPLICATIONS

Syed Saad Ahsan, Ph.D.

Cornell University 2015

Following the successes of the semiconductor industry in the 1990s, optofluidics emerged from microfluidics when the field was able to integrate liquid waveguides and plasmonic surfaces. Optofluidics is the integration of fluids and lights on the micro or nanoscale and as such is the ideal system to use for solar-chemical reactions. Due to rapid economic development and population increase, such solar-chemical reactions, whether photocatalytic or photobiological in nature, can find many applications for energy and sustainability that is investigated in this thesis.

First, we introduce a novel micro-fluidic platform to study photocatalytic water-splitting. We demonstrate how carrying out the reaction in an optofluidic environment significantly reduces the material costs and time associated with carrying out these reactions. We use this platform to study the reaction kinetics of Pt-TiO_2 which we find agreed with previous literature. Additionally, we demonstrate that such platforms have the potential to enhance the reaction rates and efficiencies by improving mass transport. To this effect, we show that simply increasing the flow

rates yielded at least ~2-fold improvements in reaction rates. We suggest that such an optofluidic platform could be used to rapidly and cheaply perform kinetic studies on different photocatalysts to screen for potential catalysts and optimize their reaction conditions.

Second, we design and fabricate light scattering waveguides that uniformly illuminate photo-bioreactors to improve growth of algal cultures. By carefully placing such scatterers on a waveguide in a gradient, we are able to achieve uniform illumination for films that are right on top of the waveguide. This gradient scattering scheme is tested along with other scattering schemes and is shown to be superior both in terms of the uniformity of growth and total coverage resulting in improvements of growth rates of 40%. Our reactors can be easily stacked to enable distribution of light efficiently when stacked in close proximity. Ultimately, we hope this will allow for these types of stacked waveguide photobioreactors to be upscaled.

Next, we build and test an integrated hollow fiber membrane stacked waveguide photobioreactor. We use a genetically modified cyanobacteria *Synechocystis* sp. PCC 6803 strain capable of producing ethylene. We are able to realize that system productivity plateaued with flow corresponding to a "gas-mixing" input energy of close to ~1W/L. In addition, at relatively high light intensities, we are able to show average to peak productivities of close to 90% for an aerated gas stream with 1% CO_2. Growth experiments at lower light intensities and higher light

intensities yield 65% and 33% improvement in plateau productivities respectively. In addition, we show a two-fold increase in growth ramp rates with carbonated gas streams, and close to 20% output improvement across light intensities in reactors loaded with high density cultures.

Finally, we demonstrate a novel photocatalytic reactor for water cleaning with augmented mass transfer and optical transfer characteristics for high-capacity applications. We use a TiO_2 sol-gel to create a porous thin film of catalyst and stack the layers closely to improve mass transport. In addition, we use light scattering waveguides in gradient formation to enable uniform illumination across the length of the waveguide. We achieve 67% degradation of the Methylene Blue dye at 10mL/min capacity and show a 4.5-5 times improvement over typical waveguide light delivery configurations. The degradation rate constant is characterized in flow rate experiments and shown to be between 0.37 – 0.54 min^{-1}. This design could in theory be upscaled for high-capacity water treatment applications.

BIOGRAPHICAL SKETCH

Syed Saad Ahsan was born in Karachi, Pakistan. He was raised in Saudi Arabia where he attended ISG-Jubail and ISGH-Dhahran. He graduated summa cum laude with a BS from the School of Applied and Engineering Physics with Honors and a BA from the Department of Economics at Cornell University in 2010. He continued his masters and doctoral studies at Cornell University, in the School of Applied and Engineering Physics, where he developed optofluidic reactors for sustainability and energy applications and received his Ph.D. degree in 2015.

In the Name of God, The Most Gracious, The Most Merciful,

Who Started His Creation with the creation of the Pen,

And His Final Instruction with the instruction to 'Read'

ACKNOWLEDGEMENTS

I would like to express my deep and heartfelt gratitude to my advisor Professor David Carl Erickson. These four years of my life could not have been possible or productive without his insight and involvement. Professor Erickson was more than an advisor; he was a confidante, a friend and a role model. I appreciate all the confidence he placed in me over these years; all the encouragement he gave; and all the praise he showered on me when I needed it (even if untrue). I learnt a lot from the way that he conducted his research with acumen and compassion and the risks he took to investigate completely new problems with faith in his students and due diligence. And I look forward to learning more in future collaborations.

I would like to thank to my previous advisor, Professor Watt Webb, for his guidance and endless support during my undergraduate years and the first year of my PhD. I feel lucky for having had the privilege to observe a great mind like his in action.

I am also indebted to my committee: Professor Jefferson Tester, and Professor Robert Jarrow for their suggestions and encouragement. It was a privilege for me to know such great minds and to receive feedback from them. I will always remember the excitement that Professor Tester had while teaching the seminar on energy and I

will always remember how to price interest rate derivatives using a model created by Professor Jarrow, one of the few things I still remember.

I have been also fortunate to have a wonderful group of friends at Cornell that includes my lab mates in the Erickson Lab; you were all like a family to me. I would especially like to thank my close friend Abdurrahman Gummus and my friends in the "Dream Team". You know who you are.

I would also like to thank my parents Syed Niaz Ahsan and Uzma Abdussalam; my sisters; nephew and nieces; and my beloved wife Tayyaba Siddiqui for their support throughout my studies. Especially my father for his intellectual imprint on me, my mother for her emotional imprint and my wife Tayyaba who lent me an ear and helped me develop some of my ideas and was a lab assistant from time to time. Without their support and love, I would not be here today.

Finally, I would like to thank God Almighty. Upon reflection, I find that somehow He has been guiding me along my journey in life. Mine is without doubt a fascinating story of how a Pakistani child can grow up in the Middle East, attending both a private Saudi middle school and a thoroughly American High School, and end up falling completely in love with a small city in upstate New York. I look forward to exploring other mysteries on my journey.

TABLE OF CONTENTS

LIST OF FIGURES

CHAPTER 1

INTRODUCTION

1.1 The Challenge of Energy and Sustainability

Global energy usage in 2008 was 474 exajoules of which more than 80% was and continues to be derived from conventional fossil fuels like coal, oil and natural gas as shown in Fig. 1.1 [1, 8]. While there are many challenges associated with the current patterns of energy consumption, the exhaustion of fossil fuel supplies is not going to occur in the short term [9]. Nonconventional sources abound. There is 5 to 10 times as much coal as conventional oil and gas while there is 5-10 times as much oil shale as coal [9]. Rather, the world may be running out of conventional sources of fossil fuels that are cheaply extractable. This means the cost of consuming energy from these sources may continue to get more costly and less reliable over time; additionally, it may not be adequate to meet the demand of energy viable for economic growth [9]. Furthermore, it is believed that current patterns of energy consumption are not friendly for the environment given the strong correlation between CO_2 emissions and global warming [10].

In order to meet the projected growing demand for energy due to population growth and economic development and keep the CO_2 concentration in the atmosphere below 550 ppm, half of all energy has to be consumed from carbon-neutral sources by 2050 [11]. This represents an absolute amount of power that is larger than all the power currently consumed. There are generally three potential technologies and modes of production that could help us meet this target: nuclear [12], carbon capture and storage[13], and renewables. While there is enough uranium to power the earth for 100 TW-years, at current power consumption rates of 13.5 TW this amounts to total time span of less than 8 years [12]. Additionally, while nuclear fusion could provide this amount of energy, the technology is not yet mature and has yet not been demonstrated [12]. Carbon sequestration could also work by dissolving carbon in underground aquifers that would not leak at rates of more than 1% a year [13]. While global reservoir capacity is sufficient to hold 100-150 years of carbon sequestration, the technology is yet not mature either [13]. Amongst renewable sources of energy that could provide and meet targets, solar could provide by far the most. More solar energy is delivered to the earth in an hour than that which is consumed in an entire year[14]. Yet because less than one percent of current energy demands come from solar, this represents a huge untapped potential[8].

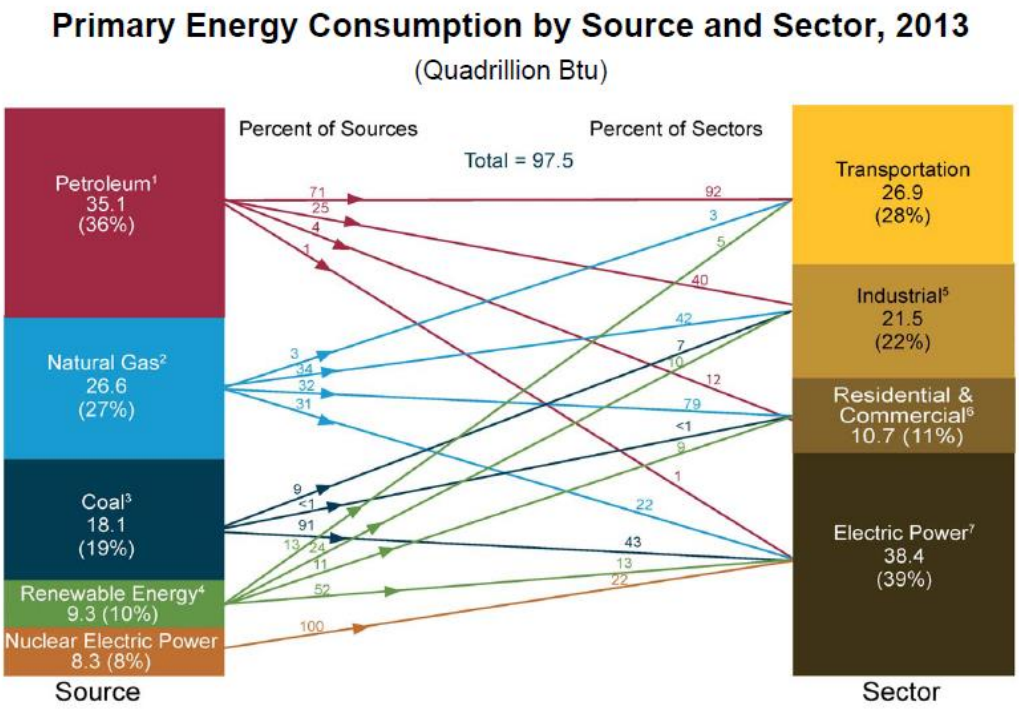

Fig. 1.1: Primary energy consumption by source and sector as reported by the US Energy Information Institute in its Monthly review. Primary energy is in the form it is first accounted for before being converted to secondary or tertiary forms. Renewable energy includes solar, geothermal, wind, biomass waste, biofuels, wood, and hydropower [1]

The use of sunlight as an alternative energy source will require its collection, storage and deployment when needed. The most common way of collecting solar energy involves the use of photovoltaic (PV) cells which convert photons into electrical currents. While the PV cells have enjoyed significant price reduction, with 90% decrease in cost over the last 30 years, they are still too expensive to compete with fossil fuel based energy production schemes[15]. Additionally the intermittent

nature of sunlight requires the need for more expensive storage and deployment mechanisms[15]. While fuel cells have been suggested, this would add another price tag to the cost of energy. On the other hand, solar chemical reactions can also utilize sunlight to produce high energy carrier molecules. This could include both hydrogen from solar water-splitting or larger biomolecules from genetically modified algae[16]. The production of such solar chemicals offers the additional possible benefit of incorporation into our current energy infrastructure without significant changes to it.

In addition, solar chemical reactions could enable other sustainable technologies and alleviate other development bottlenecks. One of the most significant of these concerns is the current need for clean water [17]. Rapid industrialization and population growth have also placed great strains on this resource and the situation is projected to exacerbate in this century [18]. One possible solution is water purification. This would entail the purification of waste water by complete mineralization of all its toxic organic compounds and the de-activation of harmful microbes [19]. Such water purification technologies have already been demonstrated using both photocatalysts and algae that can consume such waste streams.

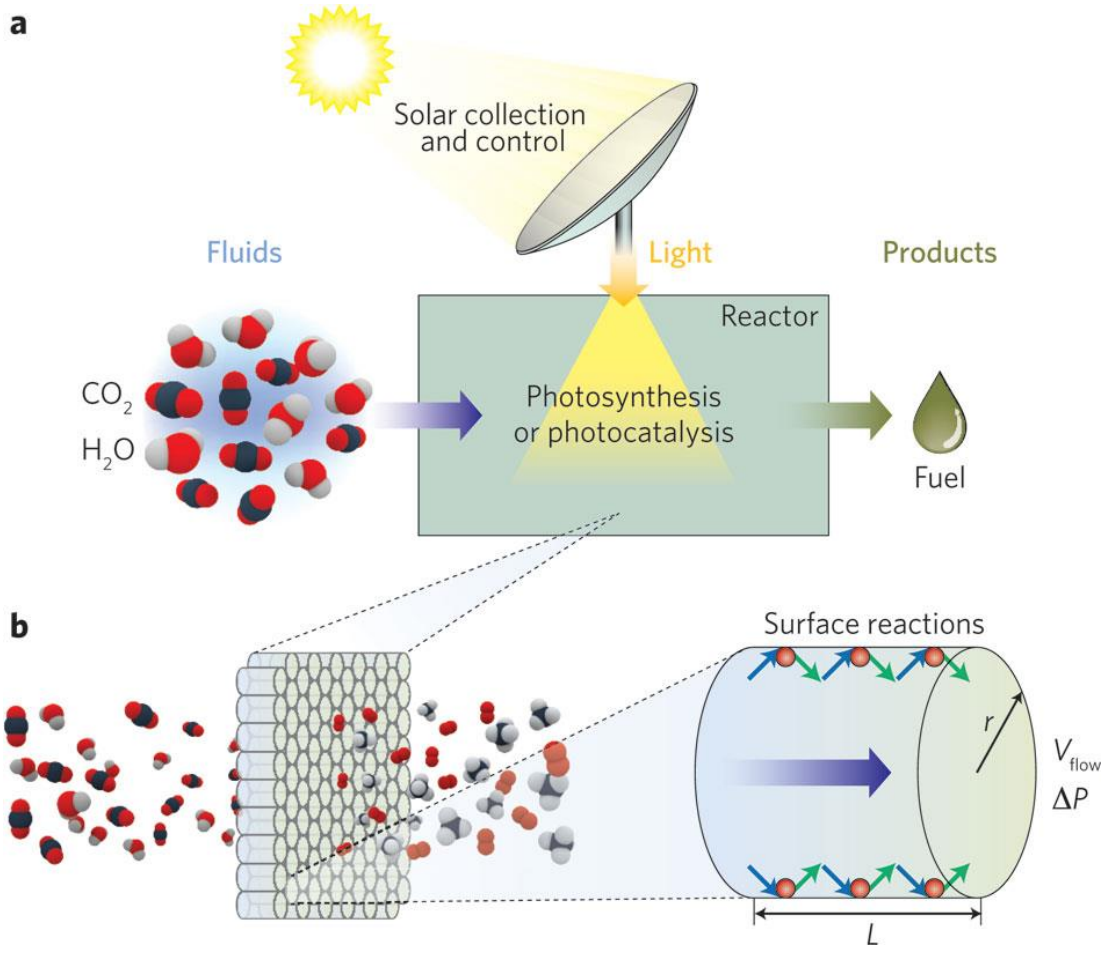

Fig. 1.2: a) Blackbox diagram for solar-chemical reactions that can include both photocatalytic or photobiological reactions, b) the relevant structures for surface driven reactions within the solar-chemical reactor. R is the radius of the reactor, L is the length of the reactor, ΔP is the gradient pressure and V_{flow} is the volumetric flow inside the micro-channel. Given parallel microchannels total capacity need not be sacrificed [5].

If one were to envision what a solar chemical reactor would entail as a black box, they would realize that it would consist of light inputs, fluid inputs and produce and waste output as shown in Fig. 1.2. This generalizes well over all such solar-

chemical reactors. Because such solar-chemical reactors entail the interplay of optics and fluidics, it is naturally an optofluidic system [5].

1.2 Optofluidics

Optofluidics is the integration of the field of microfluidics with photonics and optics [5]. Microfluidics emerged shortly after the development in the field of semiconductor devices in the 1990s [20]. Successes in the field involved the incorporation of light-guiding elements like

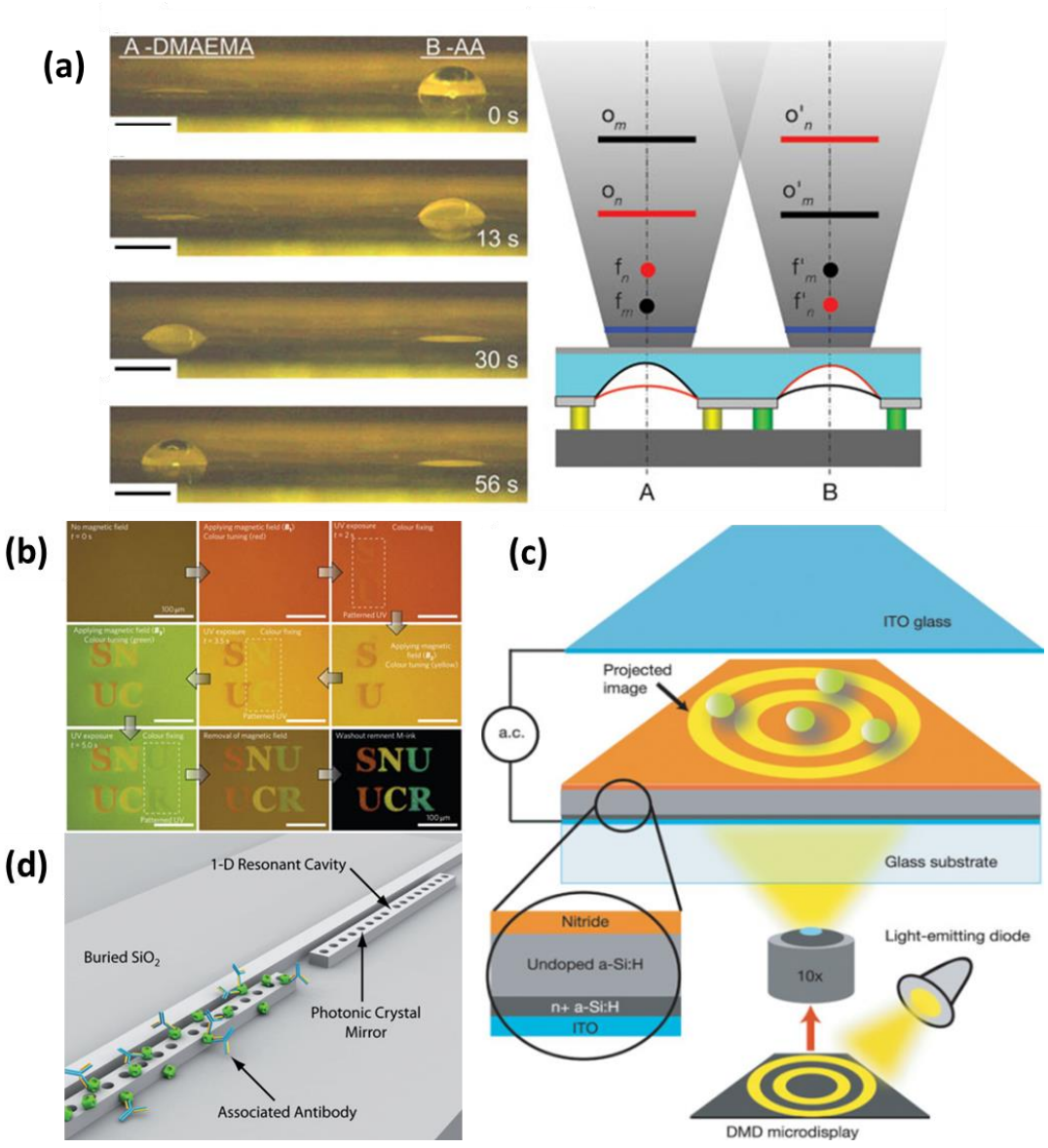

Fig. 1.3: Optofluidics enables more tunable, reconfigurable, adaptive and regenerative systems possible as shown in a) with adaptive liquid microlenses activated by stimuli-responsive hydrogels [2], and in b) with structural color printing using magnetically tunable and lithographically fixable photonic crystal [3]. It also allows for novel applications in biosensing, particle manipulation and trapping as shown in c) with massively parallel manipulation of particles [6], and in d) with optofluidic biomolecular sensors [7].

waveguides [21] and plasmonic surfaces[22]. As a result, the field of optofluidics was born. Some of its early achievements included developing ‘lab on a chip’ devices including bubble switches, liquid-crystal switchable gratings and tunable photonic crystal fibers[23]. In the mid-2000s optofluidics crystallized into an established field with novel applications in imaging, optical switching, data storage, light generation, sensing and optical manipulation[24]. One of the salient features of optofluidic technologies is its precise control of both fluidic and optical inputs. Amongst other things, this synergy has been used to improve tunability[25], reconfigurability [26], adaptability [27] and regeneration [28] of optical and photonic systems while improving biosensing [29], imaging [30], and particle manipulation[6] in fluidic systems as shown in Fig. 1.3. Recent applications include manipulation of nano-biomolecules including DNA and other nanoscale objects [31] as well as the ability to induce optically driven reactions [32].

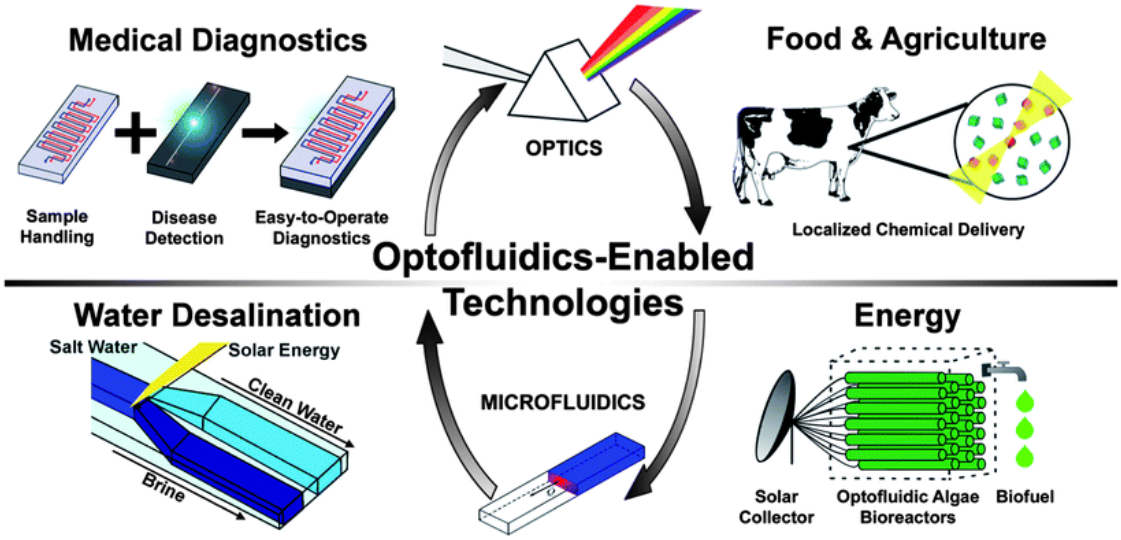

Fig. 1.4: Optofluidics has already been used for sustainability in many applications ranging from medical diagnostics in improving sample handling, disease detection and easy point-of-care diagnostics while it has also benefited food and agriculture, water desalination and purification and energy systems [5].

Amongst the reasons that optofluidic reactors are able to perform reactions more effectively is due to advantages in mass transfer and optical transfer [32]. Optofluidic environments generally enjoy large surface to volume ratios and are able to exploit many forces in the micro to nanoscale involving surface-fluid forces that allow the control and flow of fluids in very precise configurations. Additionally, the ability to direct flow in micro-channels allows such systems to benefit from much steeper gradients allowing for more pronounced mass transport at the sites of interest. As a result, the miniaturization of many reactor systems has led to several orders of improvement in reaction rates and efficiencies [33]. Of course, the control of light inputs has enabled superior performances in reactors as well[34]. This is generally

due to the more uniform distribution of light and photons and the novel methods of delivery at the points of interest.

As shown in Fig. 1.4, optofluidic reactors have already been used to enable many sustainable technologies [35]. Most of these advancements are related to medical technologies such as rapid diagnostics for diseases which involve both the detection and amplification of certain biomolecules when necessary [36]. This has led to advancements in a whole range of fields including medical diagnostics [37], animal and plant health management[38], food nutritional analysis[39], and food safety [40]. On the other hand, reactors have also been deployed to perform more complex phase transfer and chemical reactions like water purification [41] and desalination [42].

1.3 Organization of the Dissertation

Through the dissertation, we wanted to improve both photocatalytic and photobiological reactions using optofluidic environments for both sustainability and energy applications. In the Chapters 2 and 4, we investigate how to improve both photocatalytic systems for water-splitting mediated by redox carriers and high-density algal cultures in photobioreactors with ethylene producing cyanobacteria by improving their mass transfer characteristics. In Chapter 2, this is done by miniaturizing the system into micro-reactors while in Chapter 4, this is done by the use of gas permeable hollow fiber membranes. In Chapter 3 and 5, we utilize

scattering waveguides to augment photon transfer in photobiological reactors and photocatalytic water cleaning reactors. In Chapter 3, we show how to develop such scattering waveguides with gradient scatterers to enable uniform illumination to improve growth rates for planar bioreactors of *Synechocystis* sp. PCC 6803 and in Chapter 5, we use this scattering scheme to suggest designs for high-capacity reactors for water-cleaning.

CHAPTER 2

REDOX MEDIATED PHOTOCATALYTIC WATER SPLITTING IN OPTOFLUIDIC MICROREACTORS

2.1 Abstract

While photocatalytic water-splitting is a promising alternative energy source, low photocatalytic efficiencies in the visible spectrum hinders its widespread deployment and commercialization. Although screening combinations of new materials and characterizing their reaction kinetics offers possible improvements to efficiency, current experiments are challenged by expensive bulky setups and slow recovery of particles downstream. Optofluidics is a good platform for screening Z-scheme catalysts cheaply and rapidly. By alleviating the problems of mass transport it can also potentially increase reaction rates and efficiencies. Here, we demonstrate a novel optofluidic device based on applying catalyst sol-gels on planar channels while measuring the reaction output by monitoring the depletion of the redox mediators. We use our setup to study the kinetics of TiO_2-Pt water-splitting reaction mediated by I-

This work was published in *Lab On a Chip* in 2013 [43. Ahsan, S.S., A. Gumus, and D. Erickson, *Redox mediated photocatalytic water-splitting in optofluidic microreactors.* Lab on a Chip, 2013. **13**(3): p. 409-414.. All figures reproduced with permission.

/IO_3- redox pairs under different flow rates. In particular, for TiO_2-Pt, we show ~2-fold improvements in reaction rates and efficiencies.

2.2 Introduction

With fossil fuels contributing about 85-90% of the global demand for energy [44], there is dire need for alternative sources of energy that are both sustainable and environmentally-friendly. One possible alternative is the solar energy that falls on the surface of the earth. More energy arrives on the surface of the earth in one hour than the global yearly demand for energy in 2005 [45]. Unfortunately, the intermittency of solar illumination and the storage and transport of the resulting energy remains a difficult challenge. Using fuels produced by solar-chemical reactions, such as hydrogen from photocatalytic water-splitting, could replace fossil fuels with little change to current energy infrastructure and without the undesirable carbon dioxide emissions.

For solar-driven photocatalysis, the relevant variable for semiconductors is the bandgap energy which determines the wavelength above which the semiconductor will not form electron-hole pairs and thus will not catalyze the reaction, and the photo-conversion efficiency which is relevant for prospects of commercializing the technology. Some of the promising applications of photocatalysis are in water treatment [46], air pollution [47], self cleaning, disinfection [48] and water-splitting.

While photocatalytic water-splitting is not new [49], current technology has not been able to meet the stated goals of 30% quantum yield at 600nm which corresponds to 5% solar energy conversion [50].

There are many strategies to enhance the photocatalytic water-splitting efficiency and cut-off wavelength such as noble-gas doping, co-catalyst impregnation, noble-metal loading, plasmonic sensitization, and employing wire or belt-shaped geometries as described by Tong *et al.*[51]. Another popular strategy is to employ a Z-scheme system. In this scheme, oxygen and hydrogen are evolved at different catalysts, while redox mediators, such as Iodide/Iodate pairs, serve as the oxidizing or reducing agents as in Fig. 2.1.a. Because the water-splitting reaction is ultimately performed using two photons as opposed to one, the demand on each side of the reaction is lessened allowing for higher efficiencies at larger wavelengths. The highest values for quantum efficiency under visible light without using a sacrificial reagent are reported using a ZrO_2/TaON and Pt-WO_3 Z-scheme system [52].

Because optofluidics combines fluids and their interaction with light, it is potentially the optimal platform for photocatalytic reactions [5] and can increase reaction rates by improving mass and optical transfer efficiencies [32]. Additionally, by miniaturizing the reactor space, one may minimize the requirements for time, reagents and equipment. These requirements are often significant for current water-splitting setups. At present, experiments are typically run in large closed volume

setups with catalysts suspended in the solution, constantly bubbled with nitrogen gas and attached to a gas chromatograph to monitor the output products [50]. Because of the large setup, the material constraints for preparing the catalyst are not trivial. The photo-catalysts are generally recovered downstream using centrifuges and filters, washed and then reused in the setup for experiments under different conditions [53, 54]. Another advantage of optofluidic reactors is that they allow for different experiments to be conducted rapidly because the catalysts can be washed and reused for experiments with different input reagents. This allows for rapid optimization of reaction conditions and study of the kinetic properties. Additionally, while the highest reported quantum efficiencies were achieved by optimizing the reaction conditions [52], the kinetics of water-splitting reactions under a broad range of conditions has not been studied. While there have been a few comprehensive kinetics studies that have been performed on photocatalysis for exothermic reactions, such as degradation reactions [4], there have been no satisfactory comprehensive kinetic studies for truly complex endothermic reactions like water-splitting.

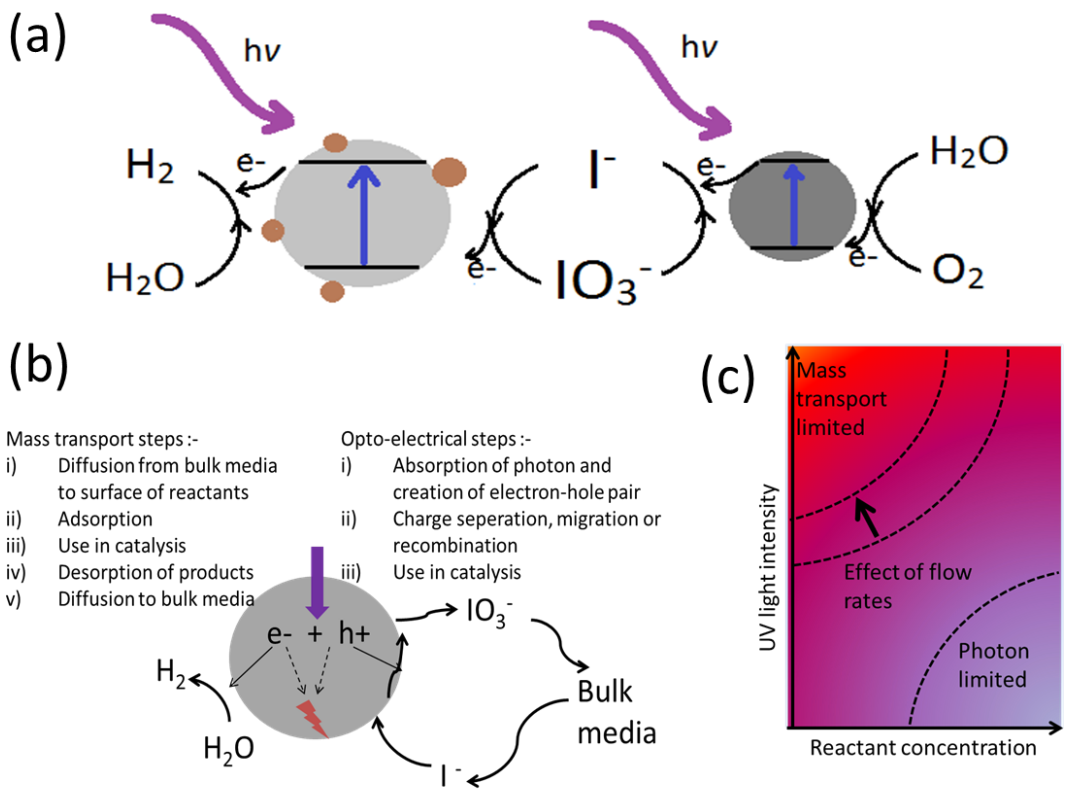

Fig. 2.1: Illustration of Chemical Reaction, Reaction Steps, and Important Kinetic Regimes. a) An illustration of a Z-scheme system where a redox mediator pair couples to the two different reactions; b) A closer look at the reaction steps. For the opto-electrical step, the photon gets absorbed creating an electron-hole pair, which either recombines or seperates and proceeds to catalyze the reaction. In the mass-transport step, the reactants and the products have to not only diffuse to the surface but also adsorb and desorb during the reaction; c) A rough sketch of the interesting kinetic regimes where the reaction is photon-limited (has the highest quantum efficiency) and mass-transport limited (where the reaction output is capped). Please refer to cited literature [4].

We can reasonably discern that all photocatalytic reactions happen in two steps [4] as in Fig. 2.1.b. In the first step, the photon is absorbed by the semiconductor particle creating an electron-hole pair which either recombines or

travels to the surface of the particle to catalyze the reaction of interest. This first-step which can be improved through chemistry and material science determines the ultimate limit of the photo-catalytic efficiency. The second step involves the removal of the products and the introduction of new reactants to the catalyst site. This mass transport step is important to ensure the adequate presence of reactants on the catalyst surface and for endothermic reactions, like water-splitting, the speedy removal of products to avoid reverse reactions. The opto-electrical transport and mass transport steps determine regimes of interest in photocatalysis which are illustrated in Fig. 2.1.c. At low levels of illumination to reactant concentrations, the reaction is photon-limited at which point it has the highest photocatalytic efficiency for a given catalyst chemistry. At high levels of illumination of reactant concentration, the reaction is mass-transport limited. Indeed, there have been many studies showing improvement of catalytic output (for reactions other than water-splitting) inside optofluidics as opposed to conventional plate and slurry reactors [55-57] due to superior mass transport. Although the improved mass transport may help in removing product gas molecules, it is hard to imagine single-photon water-splitting being mass-transport limited in aqueous solutions when the reactant is water itself; however, it is much easier to see how a Z-scheme system could potentially be mass-transport limited. Indeed, because it is not possible to improve the ultimate photon-limited efficiency by changing reaction conditions like accomplished in previous studies [52], we suggest that in Z-scheme systems improving mass transport could potentially yield significant improvements in photo-catalytic efficiency.

While others have studied photocatalysis of degradation reactions on similar optofluidic platforms [32, 58], we demonstrate the first optofluidic system to study the kinetics of photocatalytic water-splitting for TiO_2-Pt catalyst mediated by I^-/IO_3^- redox pairs. Like others [55-57], we demonstrate that optofluidics by alleviating the problems of mass transport can increase reaction rates and efficiencies. Additionally, we believe that such a platform could also allow for cheap and rapid system optimization and catalyst pre-screening. We suggest that optofluidics may not only enable higher reaction rates and efficiencies but would also be the ideal environment to study water-splitting photocatalysis.

2.3 Materials and Methods

To maximize the light-collection area, a planar reactor space was chosen. A schematic of our device is shown in Fig. 2.2.a. Our channels were fabricated using thin parafilm that could be used to create devices rapidly and bind glass to glass. We avoided PDMS as it absorbs UV light and has an insufficient elastic modulus required for stability in such a planar design. To apply the sol-gel on the glass slide, we covered the glass slide with tape and then cut out a rectangular area of 3.75cm by 1.25cm. 50µL of the sol-gel were then taken and applied to the glass slides and distributed to create a micro-film. The glass slides were then dried for 2 hours at 80°C after which they were calcinated at 550°C for 6 hours in a controlled atmosphere furnace in air to create a thin film on the surface as shown in Fig. 2.2.b.

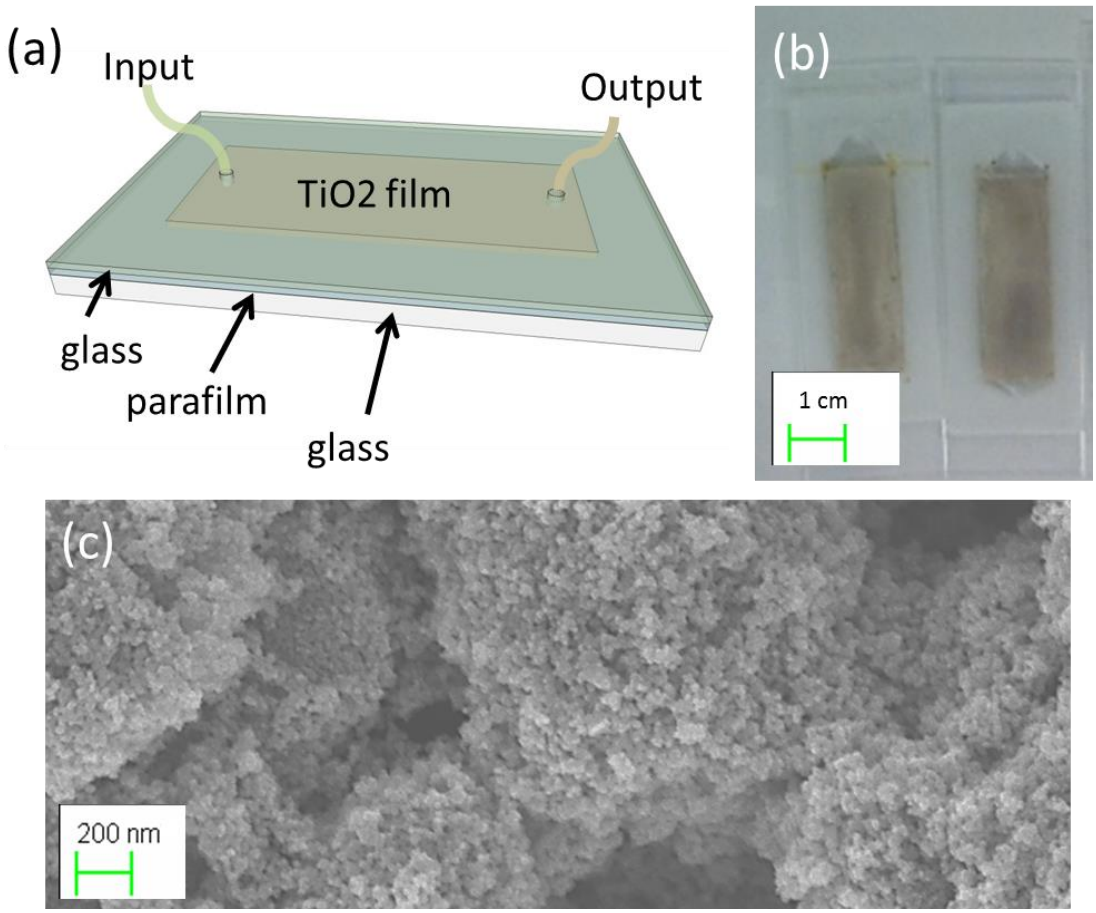

Fig. 2.2: Fabricated device, and SEM of thin film. a) Schematic of parafilm device. b) Thin TiO2 films. The two slides on the left are impregnated with Pt (0.3%). c) SEM of thin film shows porous structure with high surface to volume ratio.

To create the Pt-TiO_2 sol-gel, a dispersed colloidal suspension of platinum particles was first made by reducing hexachloroplatinic acid in borohydride in a solution with 1% PVP. The suspension was slowly dried to concentrate the Platinum particles to 70mL of solution. Then 0.23ml of acetylacetone was added and thoroughly mixed. Then 7g anatase TiO_2 nanopowder (50nm size from Sigma

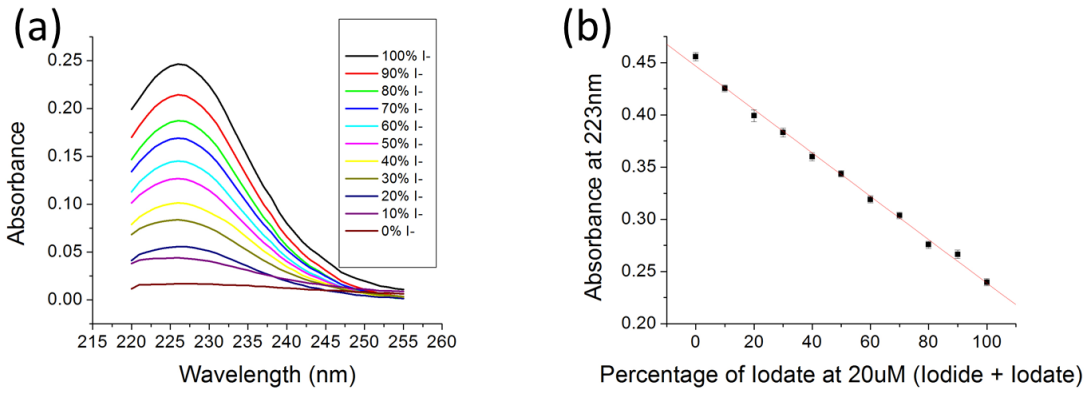

Fig. 2.3: Absorbance spectra of Iodide/Iodate and fit. (a) Absorbance Spectra at different proportions of Iodide in 20uM (Iodide + Iodate) solution normalized against buffer. (b) Using the Beer-Lambert law, A = εCl, we were able to discriminate 20uM of Iodine species of different proportions with an error of 1.4%..

Aldrich) was slowly added and mixed to disperse the powder over the solution. Then 0.2ml of a Triton X-100 was added to facilitate the spreading of the colloid after which 1.4 g of polyethylene glycol was added into the solution. The solution was then left to mix for one whole night and ready to use afterwards.

We used a 100W Hg lamp in our experiments. The input solution was kept at pH12 by adding NaOH to ensure that we would not produce tri-iodide species and to ensure that the depletion in iodine species corresponding to oxygen and hydrogen production as previously reported [59]. To calibrate the output of our reaction, we collected the output of the reaction solution in the micro-reactor both before and after we illuminated our micro-reactor with the UV light to take into account possible

contamination by displaced catalyst particles. The output samples were then taken to a UV-Vis absorption spectrophotometer where we looked at the absorption spectrum from 200-260nm. The absorption spectrophotometry fit the Beer-Lambert law in the control measurements for different proportions of Iodide to Iodate as in Fig. 2.3.a. Additionally, Iodide and Iodate have different peaks in the UV region making it possible to confirm the reaction using spectrophotometric evidence as well as in Fig. 2.3.b. All Iodine concentrations higher that 200µM were diluted to 200µM before being analyzed in the absorption spectrophotometer.

2.3 Results and Discussion

As described by others [50, 52, 59], the equations of the water-splitting reactions redox mediated by I-/IO_3- pairs are:

$$IO_3^- + 6e^- + 3H_2O \rightarrow I^- + 6OH^- \quad (2.1)$$

$$4OH^- + 4h^+ \rightarrow O_2 + 2H_2O \quad (2.2)$$

$$I^- + 6h^+ + 6OH^- \rightarrow IO_3^- + 3H_2O \quad (2.3)$$

$$2H^+ + 2e^- \rightarrow H_2 \quad (2.4)$$

Because we monitor the reaction rates via the depletion of the redox mediators, one possible limitation for our device to study photocatalysis is the requirement that the catalyst being studied is reaction specific. If the catalyst can carry out both the oxygen-producing reaction and the hydrogen-producing the reaction, then the photo-production of oxygen and hydrogen may not be correlated with the depletion of the respective redox pairs and our method cannot be used adequately. However, most catalysts that are developed for Z-scheme systems are specific for each side of the reaction and the depletion of the redox pairs is correlated with the production of oxygen and hydrogen. In addition, even if the catalyst can carry out both sides of the reaction, depletion of redox mediators may still be used if the photocatalyst is reaction specific in the kinetic regimes that are studied.

In fact, in our experiments we used a catalyst that catalyzes both sides of the reaction. However, we used information from previous studies to make sure the regimes we studied were reaction-specific. According to previous literature [59], the Pt-TiO_2 catalyst is reaction specific for the oxygen-producing reaction (1) + (2) when the concentration of iodate is high, and specific for hydrogen-producing reaction (3) + (4) (albeit with its corresponding reverse reactions) at very high iodide concentrations. As a result, the depletion of the iodine species corresponds to the production of hydrogen/oxygen in these regimes that we studied.

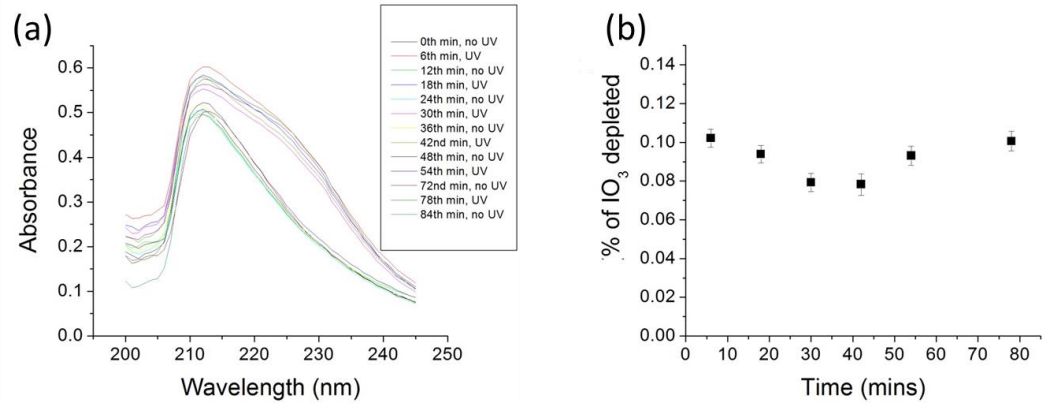

Fig. 2.4: Plots of catalytic activity over time. a) Absorbance spectrum of the output of reactor with 100uL/min flow rate for input of 200uM Iodate. UV light was toggled on and off every 6 minutes for span of 90 minutes, b) Photocatalytic activity measured by Iodate depletion in reactor. The output remains constant over entire 90 minutes period.

To assess the functionality of our microreactor, we confirmed that the reaction remained constant over a long period of time which we show in Fig. 2.4. To do this, we introduced 200µM pure iodate solution at 100µL/min over the course of 90 minutes under the presence of UV light. Our results showed that the reaction output remained constant in this period which was longer than in previous studies that found the iodine species disabled the catalyst after 30 minutes [60]. Additionally, we found that in our microfluidic chip we were able to self-clean the catalyst allowing us to change the input reagents after the cleaning and trying different concentrations or species. This showcases the advantage of carrying out these reactions in an optofluidic chip as opposed to in a bulk reactor because we could forgo the time-consuming steps of recovery, cleaning and reintroduction.

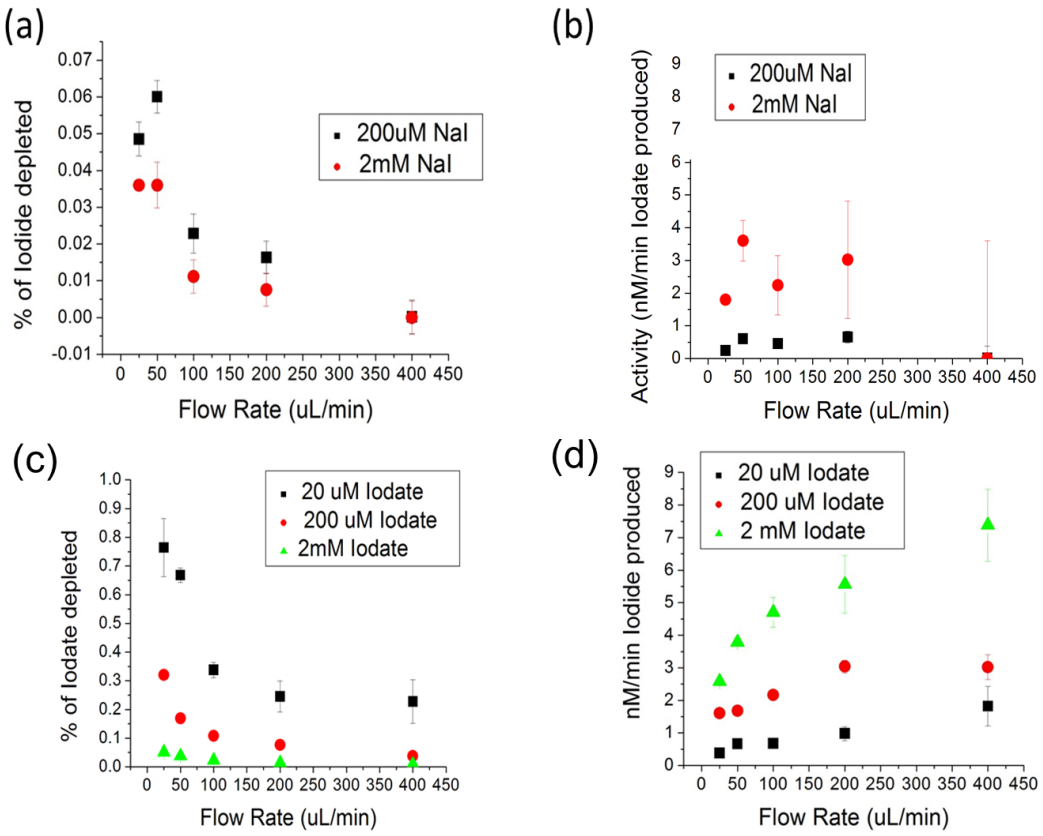

Fig. 2.5: a) and b) Photocatalytic activity for hydrogen-producing reaction in reactor. The maximum percentage converted of Iodide to Iodate is capped at 5 ± 1 %. Increasing flow rates improves output. The reaction is severely mass-transport limited at 25uL/min from 20uM NaI to 2mM NaI where activity increases proportional to concentration. c) and d) Catalytic output for oxygen-producing reaction. Increasing flow rates clearly increases output.

We also measured the reaction rates for the oxygen producing reaction under different flow rates to check for the effect of improved mass transfer efficiency. To do this, we introduced different concentrations of $NaIO_3$ solution in pH 12 to the input. Our results, shown in Fig. 2.5.a indicate that there is clearly an improvement in reaction efficiency at higher flow rates. We believe like in previous studies [32], this

is due to the improvement in the reaction rate due to improved mass transport. Additionally, we also studied the reaction kinetics of the hydrogen producing reaction under different flow rates. To do this, we introduced different concentrations of NaI solution at pH 12. We found that the output concentration was always capped such that the amount of iodide catalyzed to iodate would never increase above a certain proportion of the concentration as shown in Fig. 2.5.b. For low concentrations of Iodide, the proportion of iodide catalyzed to iodate was capped at 5 ± 1%. This agrees with results in previous literature [59] that found a high iodide concentration equilibrium presumably due to the better adsorption of the Iodate species on the Titanium Oxide surface. Syncing the two systems together shows that at comparable reaction rates, simply increasing flow rates would amount to at least ~2-fold improvement in the reaction rate and efficiency.

While mass transport can also be improved by increasing the concentration of the reactants (in our case the redox mediators) as shown here and noted in previous studies [4], there is also a visible proportional improvement across the concentrations that we studied, clearly seen for the oxygen-producing reaction, which we believe comes not from the introduction of new reactants to the catalyst site but from the removal of the products to decrease the possibility of the reverse reaction. Additionally, it is not always suitable to increase the concentration of reactants for prospects of commercialization, especially for the iodide/iodate redox pairs, due to their corrosive and toxic nature at higher concentrations.

Part of the improvement in reaction rates at higher flow rates come from improved mass transport. These improvements are consistent with previous experiments and have often been explained with the use of the following equation [32]:

$$\frac{1}{k} = \frac{1}{K * L} + \frac{1}{k_m * \alpha_v} \tag{2.5}$$

where k is the reaction rate, K is the intrinsic maximum reaction rate, L is the Langmuir adsorption coefficient, k_m is the mass diffusivity, and α_v is the surface to volume ratio. The equation suggests that part of the improvement in the reaction rates are due to improved diffusivity. This can be seen if we divide the mass transport process into two steps. The first step is the chemical adsorption/desorption of the reactant/product on the semiconductor photocatalyst while the second is the diffusive process that removes the product from the surface into the bulk media and brings the reactants to the surface of the catalyst from the bulk media as shown in Fig. 2.1.b. While the process of chemical adsorption and desorption, most typically modeled by Langmuir adsorption coefficient L, is determined by the chemical and material properties of the catalyst, the diffusive properties, modeled by k_m, can be greatly enhanced in a micro-optofluidic platform due to the presence of larger concentration gradients at even modest flow rates. Another feature that emerges is the high surface to volume ratio of these micro-reactors modeled by α_v. Indeed, previous studies have shown significant improvement in surface to volume ratios, whereas the surface to

volume ratio would be 10,000 – 30,000 m^2 /m^3 in conevntional reactors, they are <600 m^2 /m^3 in optofluidic reactors[58]. Fig. 2.2.c shows a SEM of our thin film that shows the porous nature of the thin film.

From Eq. (5) and the sorption times, one may construct a strategy to prescreen for potential catalysts which may benefit from an optofluidic platform. In particular, as long as the Langmuir adsorption rates are larger than the limiting rates given above and have demonstrated high bulk photocatalytic efficiencies, then the improvements in mass transfer efficiency and surface to volume ratios should have impact on the reaction rate. For iodide [61], radiotracer measurements have shown the adsorption and desorption constants to be 6.90 x 10^{-3} min^{-1} to 3.68 × 10^{-3} min^{-1} and 2.56 × 10^{-3} min^{-1} to 3.69 × 10^{-3} min^{-1} respectively. For iodate [62], relaxation techniques have found two different steps in the adsorption of this species onto TiO_2. Because one step is significantly slower than the latter, it is what is relevant for our purposes giving adsorption and desorption rates of 4.3 × 10^3 $mol^{-1}dm^3s^{-1}$ and 2.0 × 10 sec^{-1}. We suggest that a database of efficient photocatalysts for this reaction along with their sorption rates could be used to screen for potential candidates.

Although, there might be significant improvement from better mass transport on the nanoscale, much of the improvements from increasing flow rates may have also been achieved by changing the device geometry. In particular, for the hydrogen-producing reaction, we found that for lower concentrations of iodide (20μM NaI), the

output yielded the equilibrium proportion concentration with 5% of iodide species catalyzed to iodate regardless of the flow rates. This means that some of the improvement was due to simply reducing the residence time of the reagents in the reactor and not necessarily due to better diffusion in microfluidic environments. Reducing the lifetime of the reactants in these reactors could have been achieved through other methods, for example, by simply decreasing the volume or area size of the reactor under the same flow rate and, therefore, the average time of the reagents in each reactor bed.

2.5 Conclusions and Perspectives

In this chapter, we have used for the first time, to our knowledge, a micro-fluidic platform to study photocatalytic water-splitting. We demonstrate how carrying out the reaction in an optofluidic environment significantly reduces the material costs and time associated with carrying out these reactions. We have used this platform to study the reaction kinetics of Pt-TiO_2 which we found agreed with previous literature. Additionally, we demonstrated that such platforms have the potential to enhance the reaction rates and efficiencies by improving mass transport. To this effect, we showed that simply increasing the flow rates yielded at least ~2-fold improvements in reaction rates. We suggest that such an optofluidic platform could be used to rapidly and cheaply perform kinetic studies on different photocatalysts to screen for potential catalysts and optimize their reaction conditions.

CHAPTER 3

ENGINEERED SURFACE SCATTERERS IN EDGE-LIT SLAB WAVEGUIDES TO IMPROVE LIGHT DELIVERY IN ALGAL PHOTOBIOREACTORS

3.1 Abstract

Cultures of algae, such as cyanobacteria, are a promising source of renewable energy. Optimized algal growth occurs when the entire culture is illuminated uniformly within the useful intensity range. Most existing photobioreactors, however, do a poor job of distributing light uniformly due to shading effects. One method by which this could be improved is through the use of internal waveguiding structures incorporating engineered light scattering schemes. By varying the density of these scatterers, one can control the spatial distribution of light inside the reactor enabling better uniformity of illumination. Here, we compare a number of light scattering schemes and evaluate their ability to enhance biomass accumulation. Through a series of

This work was published in *Optics Express* in 2014 [63. Ahsan, S.S., et al., *Engineered surface scatterers in edge-lit slab waveguides to improve light delivery in algae cultivation.* Optics Express, 2014. **22**(21): p. A1526-A1537.. All figures reproduced with permission.

numerical calculations and experiments, we demonstrate a design for a gradient distribution of surface scatterers with uniform lateral scattering intensity that is superior for algal biomass accumulation, resulting in a 40% increase in the growth rate.

3.2 Introduction

One of the biggest challenges of the 21st century will be the increasing demand for energy. Between 85-90% of the current global demand for energy is met by consuming fossil fuels [44], which is not only unsustainable but also produces carbon dioxide which has been correlated with global warming [64]. While the daily energy from the sun could meet the global yearly demand for energy [45], the intermittency of solar illumination and the storage and transport of the resulting energy remains a difficult challenge [65]. Fuels produced by solar-chemical reactions, such as biofuels, could replace fossil fuels with little change to current energy infrastructure while, in principle, achieving carbon neutrality [65].

Amongst potential biofuels, microalgae represent a promising feedstock [66]. While corn, soybean, canola and palm oil are all used currently as feedstocks [67] they cannot realistically be used to completely replace petroleum-derived fuels in the near term. As described by Chisti [66], meeting 50% of current transportation fuel needs would require more than 100% of the current cropping area in the United States

using this current mix of feedstock. By contrast, algae could meet this need requiring between 1-3% of current cropping area [66].

Notwithstanding these advantages, there are many challenges associated with algal cultivation that need to be addressed to achieve cost competitiveness and large-scale commercialization [68, 69]. First of all, the energy return on investment has never been convincingly demonstrated in any large scale photo-bioreactor to be above one, which is the minimum level where energy output exceeds energy input [70]. Additionally, fuels produced by current algal cultivation are currently too expensive to be cost-competitive. According to Wijjfels and Barbosa [71], the scale of production needs to increase at least 3 orders of magnitude, with a concomitant decrease in the cost of production by a factor of 10.

A present, the most commonly used methods of algae cultivation rely on raceway ponds and tubular photobioreactors [66]. Raceway ponds have been used to cultivate algae since the 1950s and therefore there is extensive experience relating to their use and construction [66]. Nonetheless, there are also some serious disadvantages ranging from temperature fluctuations, evaporative water loss, contamination, and optical dark zones caused by poor mixing [66, 72, 73]. In contrast, because tubular photobioreactors are closed systems, they can better mitigate temperature fluctuations, water loss, and contamination. Reducing optical dark zones in these systems however typically requires active mixing which is more energetically

expensive [66, 72-75]. Generally then, although tubular photobioreactors have higher productivity, they are more expensive in terms of both cost and energy.

Development of a light delivery methodology that could overcome the limits of optical dark zones without requiring active mixing enabling and sustain high density algal cultures could help to improve the cost competiveness of the process. In highly dense algal cultures, the algae shadow themselves preventing the light from penetrating through the depth [76]. Algae growth is highly dependent on light intensity; overexposure to sunlight creates reactive oxygen species which damage the photosynthetic machinery whereas underexposure is insufficient for growth [77, 78]. Many innovative designs that incorporate larger surface areas [79], surface-plasmon-based light backscattering [80], and evanescent excitation [81, 82] to better distribute light in the photobioreactor have been previously reported.

Another method that could be employed to eliminate the optical dark zones is to use controlled light-scattering from internal waveguides [83, 84]. In this type of scheme, light is transported into the depth of the culture using waveguides where it is released into the algal culture through various scattering mechanisms. Similar methodologies have long been employed for a number of industrial applications, most notably in edge-lit LED displays [85]. As a result, there are numerous scattering schemes that have already been developed and characterized including: the use of index-mismatched materials on the surface of the waveguide, embedded nanoparticles

or other defects inside the waveguide, and shape distortions in the waveguides themselves [86-88]. Using waveguides to distribute light in bioreactors has also been previously demonstrated [81, 83, 89, 90]. Erickson *et al.* [5] proposed using of waveguiding structures to deliver light to photosynthetic organisms and microfluidics to introduce reactants and remove products [43]. Previous work has also demonstrated algae growth using evanescent excitation in optofluidic reactors [81] and using large vertically assembled slab-waveguides to scatter light into media [90]. In both of these works, however, algal growth was not uniform across the length of the reactors probably due to the decay of the intensity of the internally transmitting light in the waveguide as shown in Fig. 3.1.a.

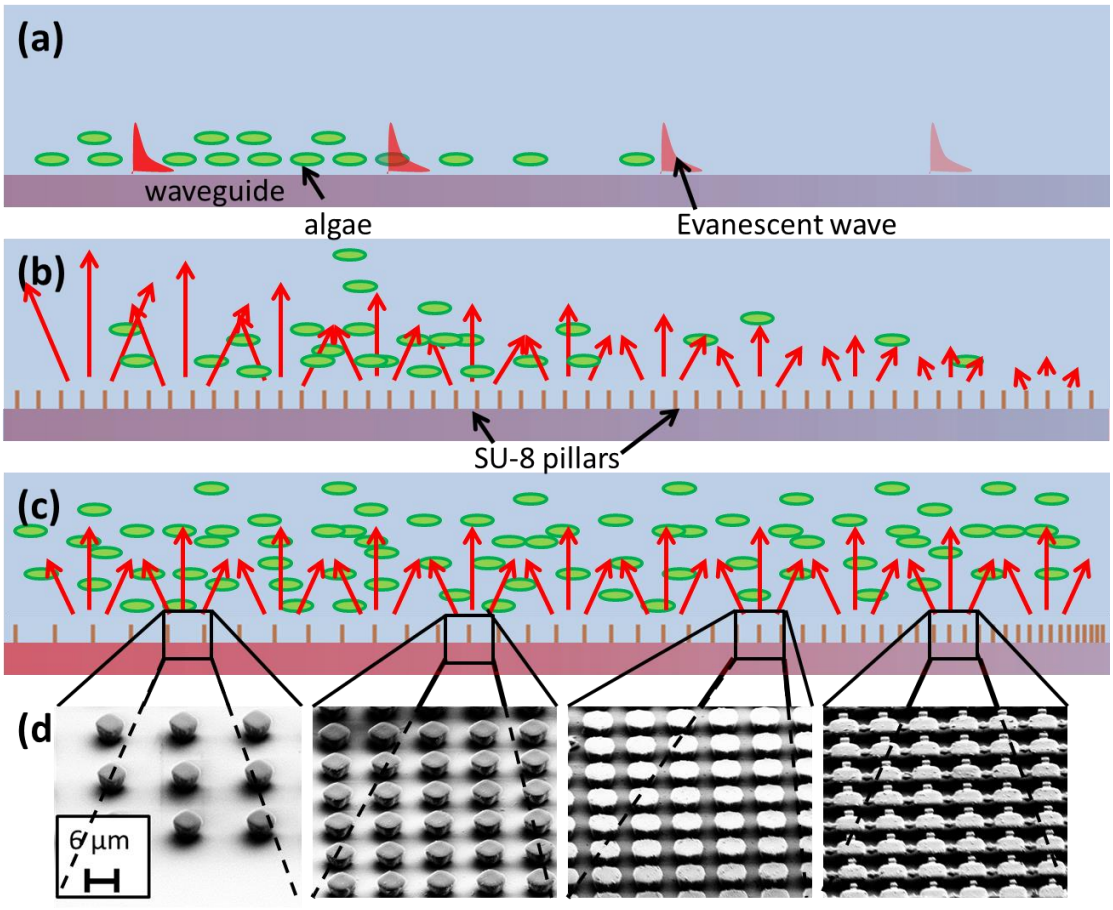

Fig. 3.1: Scatterers on slabwaveguides for algal cultivation. a) Algae can also be excited via evanescent waves where growth is confined closer to the surface of the waveguide, b) Uniform distribution of scatterers results in non-uniform illumination across the length of the reactor, c) Spatially varying the distribution of pillars results in more uniform illumination along the reactor, d) SEMs of the pillars at different densities, from left to right is variance down the length of the reactor.

In this chapter, we investigate the impact of different scattering schemes on algal biomass accumulation in bioreactors and demonstrate an illumination scheme that achieves uniform lateral illumination in the bioreactor by precisely varying the spatial distribution of light scattering pillars. We show that compared to other

schemes, this gradient surface scatterers scheme is superior for algal growth by at least 40%. In the first two sections of the results, we report how to develop this gradient scheme by first investigating the angular scattering profiles of pillars on a surface of a slab waveguide and then optimizing the lateral uniformity of illumination using a light scattering pillar scheme for a thin layer of algae by using shallow dye channels. In the final results section, we test different surface scattering schemes in a bioreactor to validate improvements in growth rates due to uniform illumination. The materials and methods are presented at the end. It is hoped that the demonstrated improvements can lead to more cost-effective high-density bioreactors with lower operational costs and reduced water and energy consumption.

3.3 Results and Discussion

3.3.1 Controlled Light Scattering Using Surface Defects

When light strikes a plane interface from a material of lower to higher refractive index, part of the light is transmitted and reflected according to the Fresnel equations. For a thin layer of a higher index material on top of the glass slab-waveguide where the angle of incidence is equal to the angle of reflection ($\theta_i = \theta_r$) and the polarization does not change, the transmission and reflectance coefficient will not change for the case of a perfectly single-mode, monochromatic wave of incidence. For periodically placed structures of the higher index material like SU-8 shown in Fig. 3.1 however, the light coupling into the pillars and back into the waveguide may be significant.

Nonetheless, as long as the coupling coefficient is low, both the intensity of the internally reflected wave and the transmitting scattered wave will decrease exponentially along the length of the waveguide.

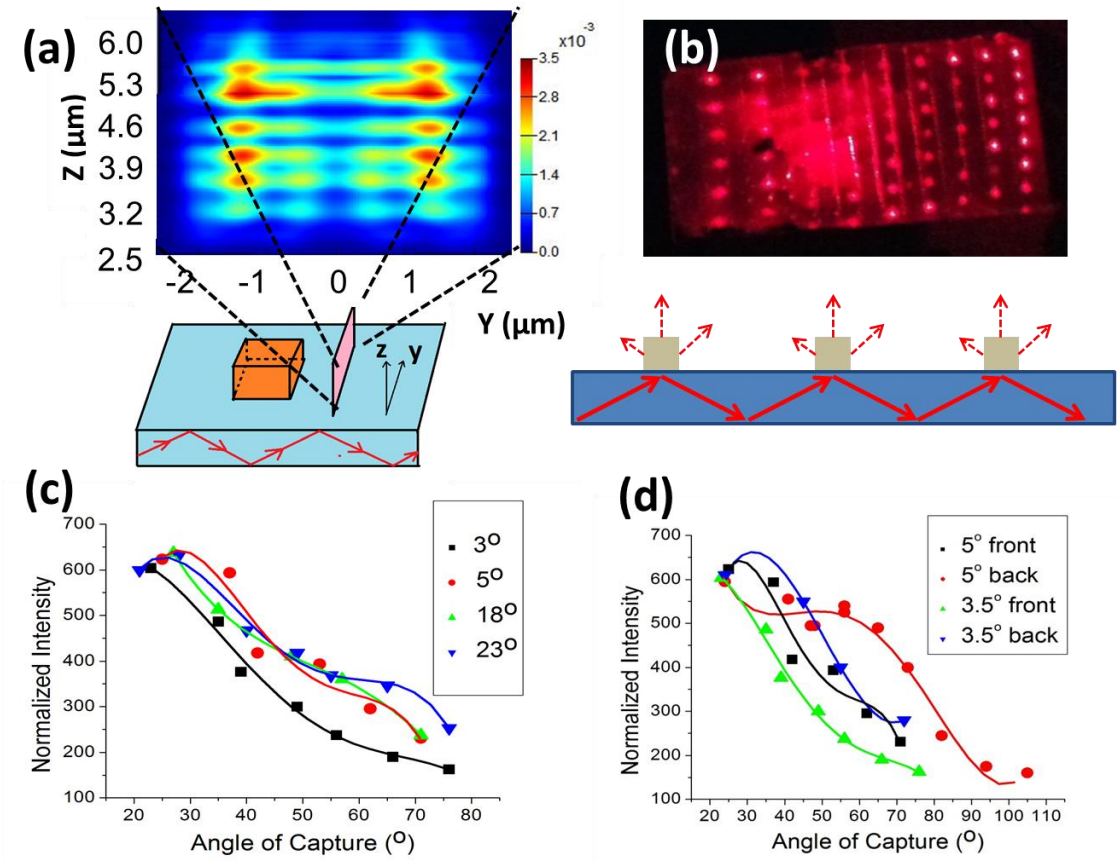

Fig. 3.2: Characterizing angular scattering from surface scatterers. a) Results from the 2D FEM simulation environment, b) periodic positions of the pillars scatter the laser light in predictable manner creating interference patterns, c) Angular scattering profiles vary with respect to the side angle of incidence of the laser, d) angular scattering profiles also seem to vary depending on the length along the waveguide when seen through pinholes at different locations from front (1cm from front edge) and back (3.5cm from front edge)

As shown in Fig. 3.2.a, simulations were performed using a finite difference time domain software package in a 2-D environment with a single SU-8 (NA=1.59) pillar on a glass surface with the incoming transmitting pane wave at five degrees. Such simulations revealed that there was negligible light that coupled into the pillars

which would couple back into the glass. Assuming that the pillar structures on the waveguide are identical, as they appear to be in SEMs taken in Fig. 3.1, and using a laser input with low divergence, we predicted and verified the presence of interference patterns on a periodic placing of pillars as shown in Fig. 3.2.b. These interference patterns were then used as a quality control when fabricating the waveguide samples with the scatterers.

Simulations also showed that even with a single pillar under a single-mode, monochromatic wave of incidence, the resulting transmitted wave had an angular profile. This angular profile would matter on the angle of incidence of the internally reflecting wave. By placing a pinhole right next to the waveguide, the angular scattering profile was empirically measured under different input angles and at two different places on the slab-waveguide. As expected, as the input angle increased, the angular scattering profile became more perpendicular to the waveguide as seen in Fig. 3.2.c. There was also some change in the angular profile along different lengths along the slab waveguide, as seen in Fig. 3.2.d which can be explained by the slight change in the distribution of the angle on incidences due to coupling into the pillar and back into glass.

For the design of an edge-lit LCD display, only the narrower range of scattering angles perpendicular to the waveguide which would be visible to an observer in the far-field need to be considered. However, in photo-bioreactors the algal culture will be in direct contact with the pillars and may have very small

penetration depth. Therefore, the design of a bioreactor which incorporates these waveguides must take into account the entire range of scattering angles. This is especially true if the input source is incoherent, multimode, and multi-angled like the LED source that is used in the following sections.

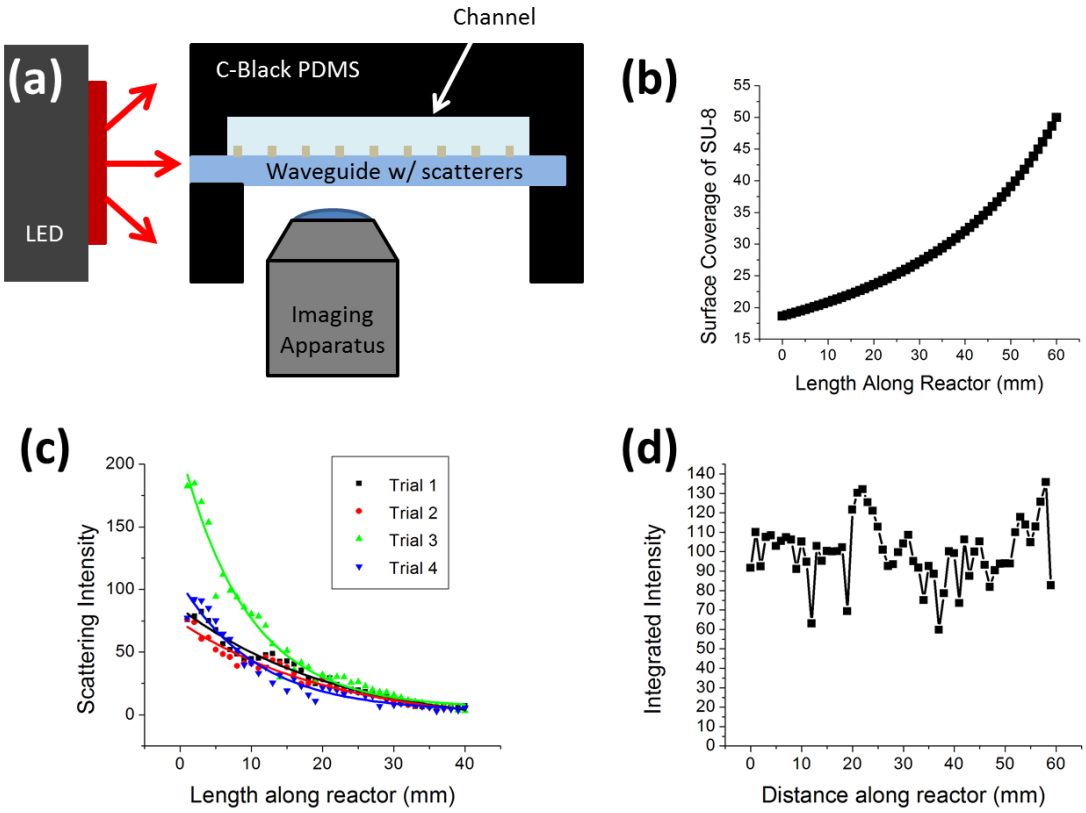

Fig. 3.3: Characterizing longitudinal scattering illumination in shallow dye channels. a) Schematic of shallow channel dye experiments, b) the surface coverage along the length of the reactor of the posts required for uniform scattering, c) the scattering along the length of the shallow dye channel when sample has uniform surface coverage of posts of 25%, d) the scattering along the length of the shallow dye channel when sample has gradient surface coverage of pillars as in 3.3.b.

3.3.2 Illumination Uniformity

In order to insure uniformity of illumination (equivalent to integrating over the angular scattering profile), shallow channel dye experiments were conducted in reactors with depths of 300 μm to simulate a thick biofilm, as shown in Fig. 3.3.a.

These experiments were conducted under conditions that were to be mirrored in the final bacteria experiments. The light scattering structures were made from SU-8, a negative photoresist commonly used in photolithography. It is reasonable to assume that each internally transmitting angle, θ, has a different extinction coefficient, $k(\theta)$ that remains constant when there is a uniform density of scatterers along the length of the reactor. It was found that even the scattering intensity of the broad-angled, and multi-mode LED source used, when integrated over the range of its various angular profiles for different transmission angles, could be well modeled with an integrated extinction coefficient, k_{int} such that,

$$S(x) = \int d\theta\, A(\theta)\, e^{-k(\theta)x} \sim A\, e^{-k_{int}\, x} \qquad (3.1)$$

where $S(x)$ is the scattering intensity integrated over the various angles along the length of the slab waveguide and A is some constant. This is illustrated in Fig. 3.3.c.

In fact, as expected the extinction coefficients were found to vary linearly with the density of scatterers present on the surface for low density surface scatterers:

$$k(sc) = k_i/sc_i \, *sc \qquad (3.2)$$

where sc is the surface coverage of the scatterers, k_i is the extinction coefficient for a sample with associated surface coverage sc_i. It was assumed that this would hold true

for higher densities of surface scatterers as well. For a pillar coverage of 25%, the associated k_{int} was found to be equal to -0.028/mm.

For a scattering scheme where the extinction coefficients can be carefully controlled, it is easy to see that to achieve uniform scattering intensity across the length of the waveguide, it should vary as:

$$K(x) = 1/(1/k_0 - x) \tag{3.3}$$

and

$$k_0 = k_{max} / (1 + L*k_{max)} \tag{3.4}$$

where L is the length of the waveguide and k_{max} is the extinction coefficient as the end of the waveguide which is also the maximum extinction coefficient. Using equations (2) and (3), one can easily derive the surface coverage of pillars required to achieve uniform scattering as:

$$SC(x) = 1/(1/k_0 - x) *k_i/sc_i \tag{3.5}$$

The highest surface coverage of pillars that was achieved was at 50% coverage. Beyond this coverage, the pillars formed a film on the glass that would peel off the surface due to poor adhesion as expected [91]. Using this as the highest surface

coverage, we were able to show relatively uniform scattering intensity across the length of the shallow channel dye reactors of 6 cm, as shown in Fig. 3.3.d using samples with gradient coverage described in equation (5) and graphed in Fig 3.3.b.

3.3.3 Improved Growth Rates in Bioreactors

After developing the scattering scheme with uniform illumination, its impact was validated on algal growth rates by performing algal growth experiments by integrating a number of different scattering schemes in bioreactors (W: 4 cm × L: 6 cm × H: 6 mm) as detailed in the Materials and Methods. First, a scattering scheme was tested with no scatterers to replicate the conditions of previous work [81] using waveguides to grow algae using only evanescent excitation. Second, there were two distinct schemes with uniform density of scatterers. This included both a waveguide with uniform pillar coverage of 50% and a waveguide with a chemically etched surface. As reported in the materials, for the chemically etched surface, an etching cream was used to etch the glass surface isotropically resulting in a uniform roughness along the waveguide. In principal, one would expect this to behave the same as a waveguide with uniform coverage of SU-8 pillars. Finally, the gradient pillar scheme was also tested.

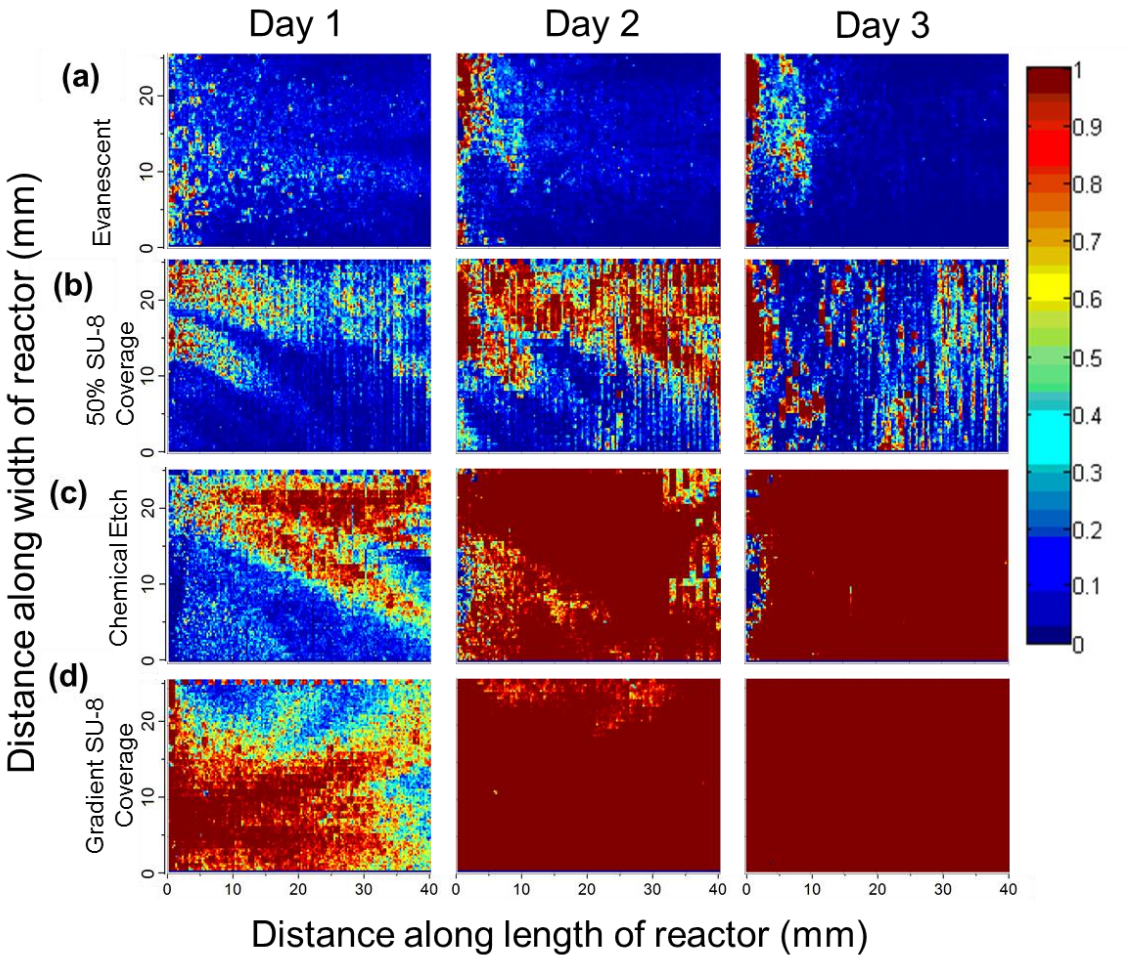

Fig. 3.4: Characterizing surface coverage of photobioreactors with different scattering schemes over the course of three days. a) evanescent excitation, b) uniform density of posts at 50% coverage, c) chemically etched waveguides, d) gradient density of pillars

The *Synechocystis* S. PCC 6803 2x EFE algal strain was used in these experiments [92]. This strain of algae is genetically modified to produce ethylene and can be more easily adopted for use inside bioreactors where it would continuously

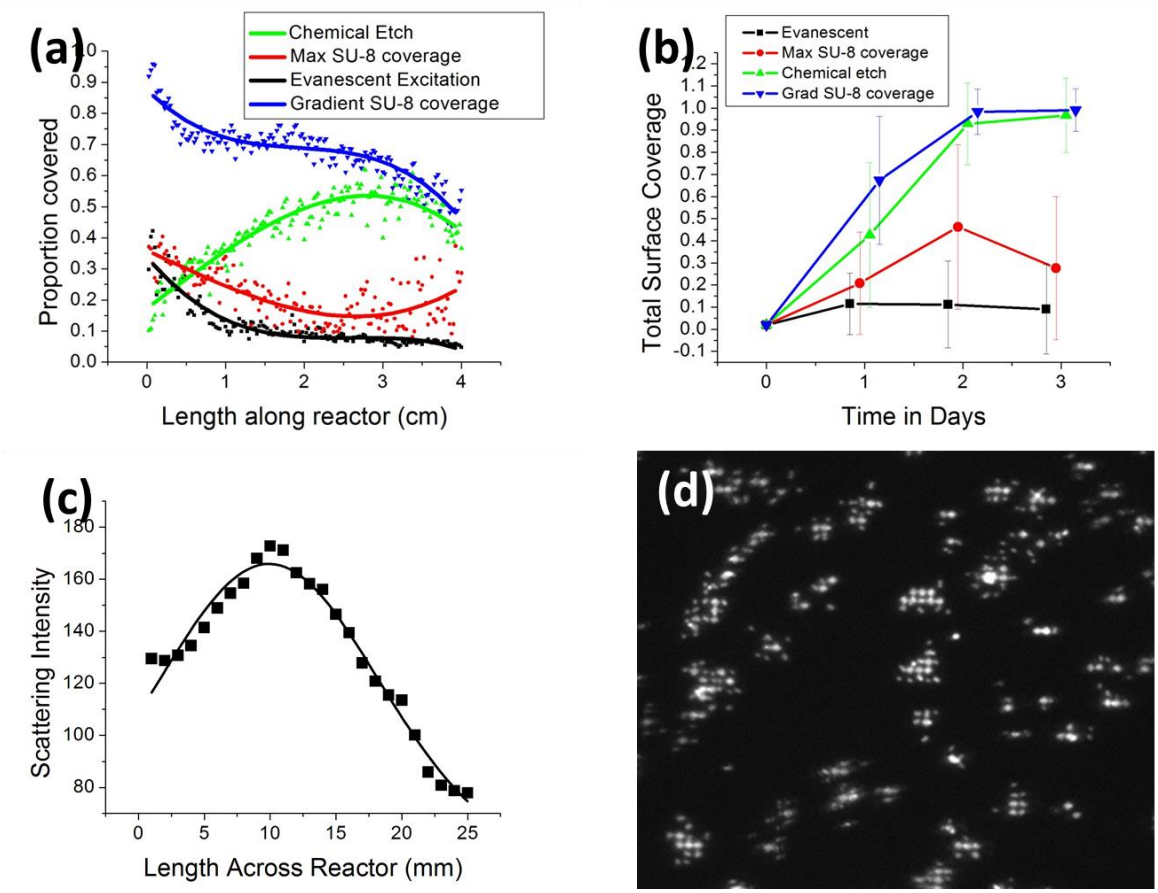

Fig. 3.5: a) The total surface coverage as a function of the length after the first day for the different scattering schemes, b) the total surface coverage for different scattering schemes over the course of the three days, c) the scattering intensity across the width of a gradient pillar sample in shallow channel dye experiments, d) a fluorescent image of the bacteria under the uniform density of posts at 50%. Notice that algal growth occurs only in between pillars and seems to be spatially confined.

produce biofuel. During the experiment, the alga tends to settle down in the absence of active mixing. Therefore, the results obtained in the shallow channel dye

experiments of the previous section should translate to these bioreactors even though they are significantly thicker.

The evanescently excitation scheme that has been used in previous papers [81] did yield significant growth of algal surfaces as shown in Fig. 3.4.a when compared to surface algal presence on the day of innoculation as shown in Fig. 3.5.a. However, as in these previous works [81], this growth was not even across the length of the reactor. The surface coverage could be modeled well with an exponential decay as shown in Fig. 3.5.a. It is possible that for this scheme, the algae themselves scatter the light such that there is, in fact, an exponential decrease in the scattering intensity. However, the relatively low index contrast between the water and the algae means that they are relatively weak scatterers that are able to transmit little light within the waveguide.

The uniform coverage of pillars at the maximum surface coverage (50%) also yielded uneven growth across the length of the algal surface, as shown in Fig. 3.4.b. This can be further seen in Fig. 3.5.a where the cumulative surface coverage across the length is graphed after one day. In fact, the scattering intensity should have a steep extinction coefficient, and because algal growth is highly dependent on the light intensity, this is not a surprising result. This uneven surface coverage seems to spread out at longer times. This is likely because of the poor settling of the algae on the surface with such high SU-8 surface coverage. Fig. 3.5.d illustrates that the algae seem to settle only in between the pillars. This may be due to the hydrophobic nature

of SU-8. It is possible that there may be significant portion of the algal culture that was not allowed to settle on the surface violating the assumptions made to relate these reactors to the results derived in the shallow channel experiments. This could make the algal growth in this reactor grow in patches with spatially constrained colonies.

As shown in Fig. 3.4.c, the scattering scheme with chemically etched surfaces demonstrated strong growth over the course of the three days eventually spreading to cover the entire reactor. However, as shown in Fig. 3.5.a, the growth on the first day reveals that there are uneven growth characteristics over the length of the reactor. Because the chemically etch treatment was the same across the length of the reactor, the scattering properties should be similar yielding a illumination intensity that decreases exponentially along the length of the reactor. Because algal growth is highly dependent on light intensity, this creates an optimal zone for growth while the intensity outside of this zone is not suitable for growth. However, the growth is quite strong and the algal cultures do spread out to cover the entire reactor over the course of the three day experiment.

The gradient coverage of pillars yielded the strongest growth over the course of the three days eventually covering the entire surface as shown in Fig. 3.4.d. In these experiments, the density of pillars varied from 19% at the leading edge to 32% at the end. There does seem to be slight indications of uneven growth after the first day of growth but this may be explained by the disinclination of the algae to settle at higher SU-8 densities and possibly by slight variations in the empirical determination

of the extinction coefficient in different samples of uniform coverage of pillars in the shallow channel dye experiments. Nonetheless, it is clear that the gradient coverage is uniquely superior to the other scattering schemes, both in relative uniformity of algal surface coverage and the growth of the surface coverage throughout the reactor, as seen in Fig. 3.5.a and Fig. 3.5.b.

The surface coverage growth, shown in Fig. 3.5.b, was fit to a logistic function, in equation (6), to extract the characteristic growth rates of each scattering scheme:

$$P(t) = K*P_0e^{rt}/(K + P_0(e^{rt}-1)) \quad (3.6)$$

where K is 1, and P_o is 0.07 or the initial surface coverage of the chip. The equation fits the data very well especially for the chemical and gradient coverage scattering schemes. It also reveals that there are significant differentials in the growth rates for each scattering schemes. The doubling times for the algae in the total chip for the evanescently excited, maximum pillar coverage, chemically etched, and gradient pillar schemes were 4.34 days, 0.95 days, 0.29 days and 0.21 days respectively. The fastest growth rate was that of the scheme incorporating a gradient distribution of light-scattering pillars which had uniform intensity and showed a 40% increase in growth rate as compared to the chemically etched scheme with uniform surface roughness profile but non-uniform scattering intensity.

There also seems to be significant variations in the growth of the algae across the width of the reactor. In all the reactors, it seems that growth is stronger in portions near the center. Indeed, this is also an expected result as we did not control for the variations across the width of the reactor. This variation in scattering intensity across the width of the reactor is a result of the fact that the panel of LEDs used to illuminate the reactor was smaller than the width of the waveguides. Of course, this is a problem with an easy solution if the center of the LED panels is aligned with the reactor and the variation in the scattering intensity across the width of the reactor is characterized as in Fig. 3.5.c and controlled by varying the surface coverage across the width. While this work employed SU-8 pillars as the surface scatterers, there are industrial alternatives that are easier to employ and cheaper to produce such as hot embossing. These industrial alternatives could make producing such waveguides for algal cultivation mass producible allowing for the potential of competitive photo-bioreactor technology if up-scaled.

3.4 Materials and Methods

3.4.1 Fabricating Waveguide Samples

1 mm borosilicate glass slides were cleaned with soap, and then soaked in nanostrip for 10 minutes. Then, glass slides were heated for 30 mins at 200℃ on a hot plate. SU-8 2002 (Microchem) was spun on first at 500 RPM with 250r/s acceleration for 10 seconds then 1000 RPM with 500r/s acceleration for 30 seconds to achieve a 2.8

micron thick layer. Next, slides were placed on a hotplate at 95℃ for four minutes. SU-8 was exposed for seven seconds using hard contact exposure on the Suss MA6-BA6 Contact Aligner. Afterwards, slides underwent a post exposure bake at 95℃ for two minutes. SU-8 was developed in SU-8 developer for one minute. Finally, they were rinsed off with IPA and dried with nitrogen. The 25% uniform coverage waveguides were made by patterning an array of 5 μm by 5 μm pillars spaced 5.0 μm apart on the glass (Fig. 3.1). Gradients of different percent coverage at each mm along the glass were constructed by changing the spacing between the pillars. To fabricate the chemically etched waveguides, a glass etching cream from Armour Etch was purchased. The etching cream was then applied to the glass slide for seven hours after which the glass slide was soaked in water and the etching cream was washed away.

3.4.2 Characterizing SU-8 Surface Scattering

Simulations were performed in a 2-D FEM environment simulation. The Environment consisted of one SU-8 pillar on glass where the internally transmitted light had an angle of 5 degrees with respect to the surface of the glass. The wave was modeled as a plain wave inside the glass.

The scattering experiments were conducted using a SU-8 sample prepared on a coverslip. The SU-8 surface was concealed with a coverslip covered with black tape except with a pinhole either 1cm or 3.5 cm from the input edge of the slide. A diode laser (Newport LPM660-30C) was used to illuminate the edge of the slide at varying

input angles with respect to the surface of the glass slide. The scattering intensity was captured with an optical power meter (Thorlabs PM100D) in a black room at a constant angle of several inches in the altitudinal plane of the laser. The capture angle was varied to measure the cross section of the scattering in the altitudinal plane.

3.4.3 Shallow Channel Dye Experiments

Chambers designed to hold florescent dye, with dimensions of 40 mm X 60 mm and depth of 300μm were constructed using the waveguide for the top of the chamber. A mixture of 1:100 carbon black to Polydimethylsiloxane (PDMS) was poured over a mold the dimensions of the SU-8 coverage, and placed in a 90°C oven for 30 min. The molded PDMS formed the base of the chamber and was bonded to the waveguide. Next, a small slit was cut in a black tin foil sheet and the glass was inserted. The tinfoil was also bonded to the glass by placing the same black PDMS around the slit sealing it off as to only allow light into the glass. The chambers were filled with Alexa Fluor 680 dye (Life Technologies). The short edge of the chamber was placed 10 mm away from the center of a 10 X 10 array of LEDs, emission wavelength ~630nm, spaced 2 mm apart. A fluorescence image of the dye was taken around 700nm, at 10x magnification, with a Sony XCD-X710 Firewire Camera attached to a microscope. An image was taken over the length of the chamber every 1 mm. The average pixel intensity of each image was extracted and plotted on a graph.

This data was fit to an exponential curve to determine the exponential decrease coefficient.

3.4.4 Algal Bio-Reactors

The *Synechocystis* S. PCC 6803 2x EFE ethylene producing strand was kindly provided by NREL. It was maintained in carbonated BG-11 media and regularly inoculated to keep it in its exponential phase under a yellow fluorescent lamp at room temperature. The PDMS chambers for the bacteria were fabricated using a laser-cut plastic master (*W*: 4 cm × *L*: 6 cm × *H*: 6 mm). A mixture of 1:100 carbon black to Polydimethylsiloxane (PDMS) was poured over the plastic mold and cured at 80°C oven for 60 min. The PDMS chamber was then bonded to the scattering waveguides to form the final chamber. The sides of the waveguides, except for in the front, were then coated with black PDMS, as well, to block the entry of light from the sides. On the bottom of the waveguides, a grid mm^2 boxes was also attached. To create the initial surface coverage, reactors were inoculated with 1:100 dilution of the culture at OD_{750} of 0.1 through the PDMS top using a syringe. The chambers with the different scattering schemes were placed 10cm away from the center of a 10 X 10 array of LEDs of emission wavelength 630nm. During the course of the illumination, the chambers were placed on a glass slide covered with black tape.

3.4.5 Imaging and Analysis

The experiments were carried out for three days. We had four different scattering schemes: evanescent excitation, chemically etched scattering, scattering with a uniform surface of 50% SU-8 coverage and a gradient coverage with maximum coverage at 32%. Images were taken through the bottom of the waveguide using at 10x magnification, with a Sony XCD-X710 Firewire Camera attached to a microscope. To analyze the images, we used the same method as reported by Kalontarov et.al. [93], which gave us information on the surface coverage in each square grid. The thresholding parameter used to distinguish between the presence of an algal surface, or lack thereof, was set as the same for the images in each scattering scheme. Surface coverage information was then extracted over an area of 25mm by 40mm for each reactor.

3.5 Conclusions

In this chapter, we designed and fabricated light scattering waveguides that uniformly illuminated photo-bioreactors to improve growth of algal cultures. This gradient scattering scheme was tested along with other scattering schemes and was shown to be superior both in terms of the uniformity of growth and total coverage resulting in improvements of growth rates of 40%. Our reactors can be easily stacked to enable us to distribute light efficiently when stacked in close proximity and are compatible with

genetically modified strains that could produce biofuels directly. Ultimately, we hope this will reduce the maintenance and harvesting costs biofuels from photobioreactor.

CHAPTER 4

STACKED OPTICAL WAVEGUIDE REACTORS WITH INTEGRATED HOLLOW FIBER MEMBRANES FOR HIGH-DENSITY ALGAL CULTURES

4.1 Abstract

In this work, we present a compact algal reactor with stacked layers of waveguides with scatterers to better distribute light and hollow fiber membranes to better facilitate gas transfer. Previous stacked waveguide algal reactors built in our group have achieved 8-fold improvement in biomass productivity, carrying capacities of OD_{730} 20; and fuel production rates four times that of flat-plate reactors. Here, we further optimize these reactors by integrating hollow fiber membranes to alleviate bottlenecks associated with carbon depletion and oxygen build-up. We achieve close to 65% improvement in plateau peak productivities under low light intensities growth experiments while maintaining 90% average/peak productivity output over the course of 7 hour light cycles. With an associated mixing cost of ~1W/L, we show a two-fold increase in growth ramp rates with carbonated gas streams under high light intensities, and close to 20% output improvement across light intensities in reactors

This work was supported by the Advanced Research Project Agency – Energy.

loaded with high density cultures leading to max productivities in excess of 1200 μg L^{-1} h^{-1}.

4.2 Introduction

Energy is one of the most pressing challenges of the 21st century. Amongst potential sources of alternative energy, there has been considerable interest on biomass from algae. Algae are seen as a promising feedstock due to their high areal/volumetric productivity [66, 94, 95], independence from arable land [71, 96] and from fresh water in some species [97], non-competition with conventional food crops [96], potentially fast growth rates with high oil content [98], the ability of absorbing/treating waste streams rich in carbon, nitrogen and phosphorus [99-101], and the possibility of producing high-value food and pharmaceutical co-products [72, 102].

The most common method to cultivate algae involves the use of circular raceway ponds [66]. These are the most common choice due to low capital costs [103]. Because raceway ponds are open system, they are vulnerable to large amounts of water loss and unwanted contamination [66, 72, 73]. In addition, they are unable to distribute nutrients like CO_2 and remove wastes like O_2 uniformly due to poor mixing in such large ponds [72, 73]. Another deficiency is the non-uniform distribution of light in the bio-reactor. Algal growth is highly dependent on light intensity and peak sunlight intensity is too high for optimal algal growth; as a result, the top layer of the

algal culture is photo-inhibited which destroys their photo-synthetic machinery by creating radical species [77, 78]. The algae self-shade so that only a thin layer of the pond receives the optimal light intensity while the bottom layer does not get enough light to sustain growth [76]. In contrast, while closed photobioreactor (PBR) systems, like tube reactors and flat-plate reactors are expensive in capital cost, they are able to offer better control over water loss, temperature fluctuations and unwanted contamination [103]. Unfortunately, they also suffer from poor light and nutrient distribution due to self-shading effects in dense algal cultures [66, 72, 104]. To overcome these effects to achieve high-density cultures requires energy-intensive mixing to cycle individual algae to the optimal light zones from the non-optimal zones, and to better distribute carbon dioxide and remove oxygen [66, 72-75]. Even in simple closed PBR systems, the energy required for mixing is close to the energy that is eventually harvested from the system [97]; therefore, the energy return on investment (EROI), a measure of energy input versus output, is very low for such systems and has not been convincingly shown to be greater than one [105]. Furthermore, the cost of mixing amounts to a significant 13% to 52% of total construction and operation costs [106].

To address these problems, previous publications in our group have developed compact waveguide photobioreactors to address the light distribution in closed PBR systems [81]. By delivering light through the side of the waveguides where it is transmitted throughout the waveguide via total internal reflection, the light can be released into the culture through embedded scatterers [63]. In addition, stacking such

systems closely to reduce the light path between each parallel waveguide enables near-uniform light distribution throughout the culture volume [107]. The use of such compact stacked scattering waveguide (SW)-PBRs has enabled up to 8-fold increase in bio-mass productivity and enabled the possibility of sustaining high-density algal cultures [108]. Previous works have optimized such SW-PBRs systems achieving a carrying capacity of OD_{730} 20 [108]. Additionally, they have demonstrated the integration of this system with a genetically modified algal strain capable of secreting ethylene that would simplify post-processing steps including harvesting and product extraction that conventionally account for 50% of total production cost [107, 108]. Such SW-PBRs also managed to improve ethylene production rates to 937 $\mu g\ L^{-1}\ h^{-1}$ which represented a fourfold improvement over a conventional flat plate PBR [108].

Previous SW-PBRs built did suffer from bottlenecks due to gas nutrient exchange. Because the SW-PBRs were closed systems, the production of product and waste gases expels a portion of the algal culture daily. In high density cultures, there is a particularly strong need for high-gas exchanges because of the high volumetric reaction rates; adequate CO2 needs to be supplied while oxygen needs to be constantly removed to avoid toxic conditions. One possible strategy to accomplish this is through the use of hollow-fiber membranes (HFMs) for gas exchange [109]. Previous works have demonstrated the efficacy of HFMs for gas-exchange in sustaining algal cultures [109, 110]. Single-stack reactors integrated with HFMs developed culture surface densities of nearly 90% which remained constant for 17 days [109]. In addition, actively aerating the fibers by pumping atmospheric air

through them showed both an increase in the specific growth rate by 15% and the average surface density by 35% when compared to a passive aeration scheme [110]. It also managed to eliminate any gradients along the length of the fibers [110]. While pumping air through HFMs will require some energy input, it should be a fraction of that of pumping liquid media through reactors which have both higher densities and viscosities.

In this short communication, we build and investigate hollow-fiber membrane stacked waveguide photobioreactors (HFMSWPBRs). The hollow fiber membranes are used to alleviate oxygen build-up and deliver carbon dioxide while removing ethylene which is collected at the output to determine system productivity. We investigate the reactor performance under three different input gas stream conditions: - passive flow, active flow with room air, and active flow with carbonated air. We show that compared to simple SWPBRs, their HFM counterparts have significantly greater photosynthetic-efficiency in producing ethylene while consuming on the order of ~1W/L for aeration energy which is significantly smaller than conventional reactors. In addition, active aeration improves steady-state ethylene production significantly by 35% under high light intensity and even at low light intensities by over 60%. In addition, we show that integrating hollow-fiber membranes also allow higher production capacities in high OD experiments over the breadth of light intensities.

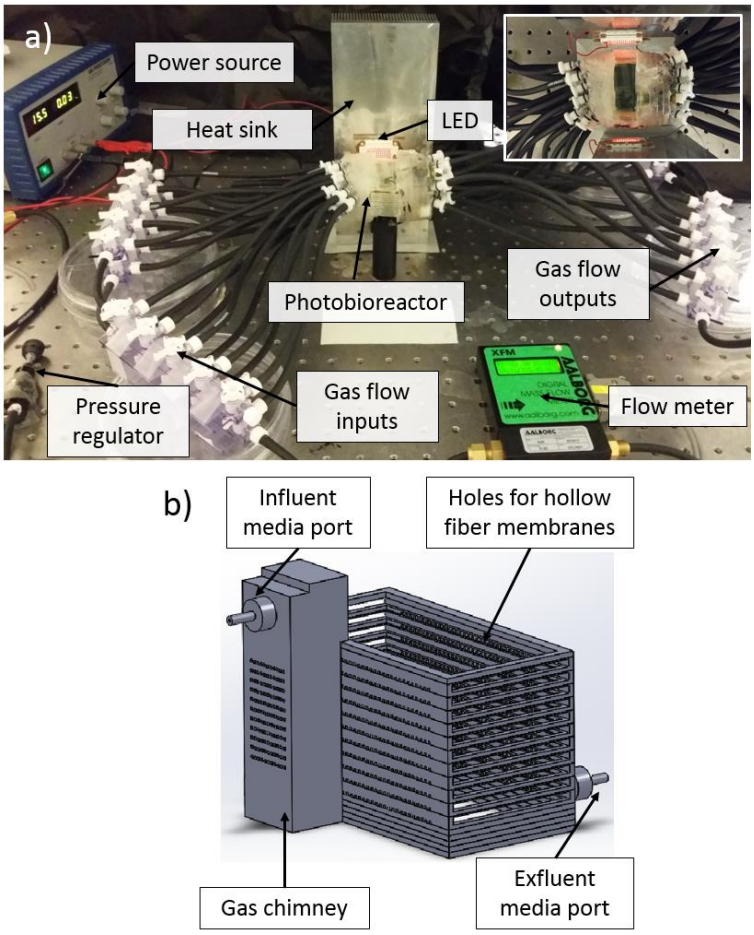

Fig. 4.1: a) The system setup includes the power source, pressure regulator, pressure source (not shown), the gas flow inputs, the photobioreactor, the gas flow output, the flow meter, the LED banks and the heat sink. b) the 3D print design of the hollow fiber membrane reactor includes influent and effluent media ports, holes for hollow fiber membranes in each of the 10 slots for the waveguides.

4.3 Methods and Materials

4.3.1 Reactor Design and Assembly

The reactor frames were printed using a 3D printer with a photocurable resin (VeroClear, Objet Geometries Inc.). As shown in Fig. 4.1.b, the dimension on the frame was 7.5 cm x 2.5 cm x 3 cm (length x width x height). The reactor frames consisted of 10 parallel slots reactor separated by 2mm along the height of the reactor for each waveguide. In addition, there were holes separated by 1mm in each waveguide layer for hollow fiber membranes (model no. MHF304KM purchased from the Mitsubishi Rayon Co., Ltd.) to be placed to transverse along the width of the reactor where they were bunched through nozzles on each layer for easy gas delivery and removal. The reactor had a chimney connecting each waveguide layer to better allow fluid transport between layers and two ports: - one for influent media on the bottom and one for effluent media on the top. After assembly of the reactor frame with the waveguides and hollow fiber membranes, Polydimethylsiloxane (PDMS) (Dow Chemicals, Midland, Michigan, USA) was used to fix all the parts in place including the fibers and their nozzles and then coated with parylene C to ensure airtight conditions.

4.3.2 Waveguide Fabrication

Waveguides were fabricated on 1mm borosilicate glass slides. The glass slides were coated with a glass-etching paste (purchased from Armour Etch) for 7 hours to produce isotropically etched surfaces with a characteristic roughness to randomly scatter the internally transmitted light. The slides were then affixed with 80 um

coverslips and sealed in place with PDMS to create air cladding at the interface to better scatter the light. The light intensity was determined from having control SWPBRs using methods reported by previous work.

4.3.3 Organism

A genetically modified blugreen algae strain of cyanobacteria Synechocystis sp. PCC 6803, was used for experiments and served as the model organism. Semibatch cultures were cultivated for the inoculum in the PBRs in flasks and maintained in their growth phase at OD 730 of 1-2. The culture media consisted of standard BG-11 medium (5x), 20mM NaHCO3 as an additional carbon source, 4.6 g/L TES buffer, 25mg/L spectinomycin and 200mg/L kanamycin. The antibiotics were used to ensure that the modified strain resistant to antibioitcs would not revert to its wild-type strain.

4.3.4 Experimental Conditions

Fig. 4.1.a illustrates the main components in the experimental setup. The reactors were illuminated during the light cycles by LED banks placed on both sides of the reactor about 1 cm away. The light was delivered through the side of the glass slides and released into the culture volume in a relatively uniform intensity distribution. The reactors were run for 6-8 hours of light cycles each day depending on the pH of the culture volume. If pH increased beyond 9.5 in a particular run (indicating carbon-

limited conditions), the light cycle hours were reduced to alleviate this problem. The algal volume was removed from the bioreactor each day, centrifuged, and re-suspended in fresh media each day to ensure the presence of a carbon source in the media besides what they may have received from the gas flow. Unfortunately, because of the close packing of the fibers in the system, it was hard to remove all the culture to get an idea of the culture health through the OD. Instead to get an idea of system productivity and growth, we used the increase in system ethylene productivity.

4.3.5 Gas flow and sampling

During the experiment, we investigated three different gas stream flows:- passive flow, room air flow and flow with 1% CO2 in air (Airgas). Because a measurement of the system production required active aeration, we started the runs with active flow for the first hour at the end of which we would collect several mL of gas as the gas sampling port. These measurements would give us an idea of system peak productivity that we collected for the growth rate data. For the passive flow runs, the aeration would then be closed for the rest of the day to best approximate SWPBR systems. For the room air flow runs and flow with 1% CO2 in air, we continued the flow with room air till the end of the light cycle.

4.4 Results and discussion

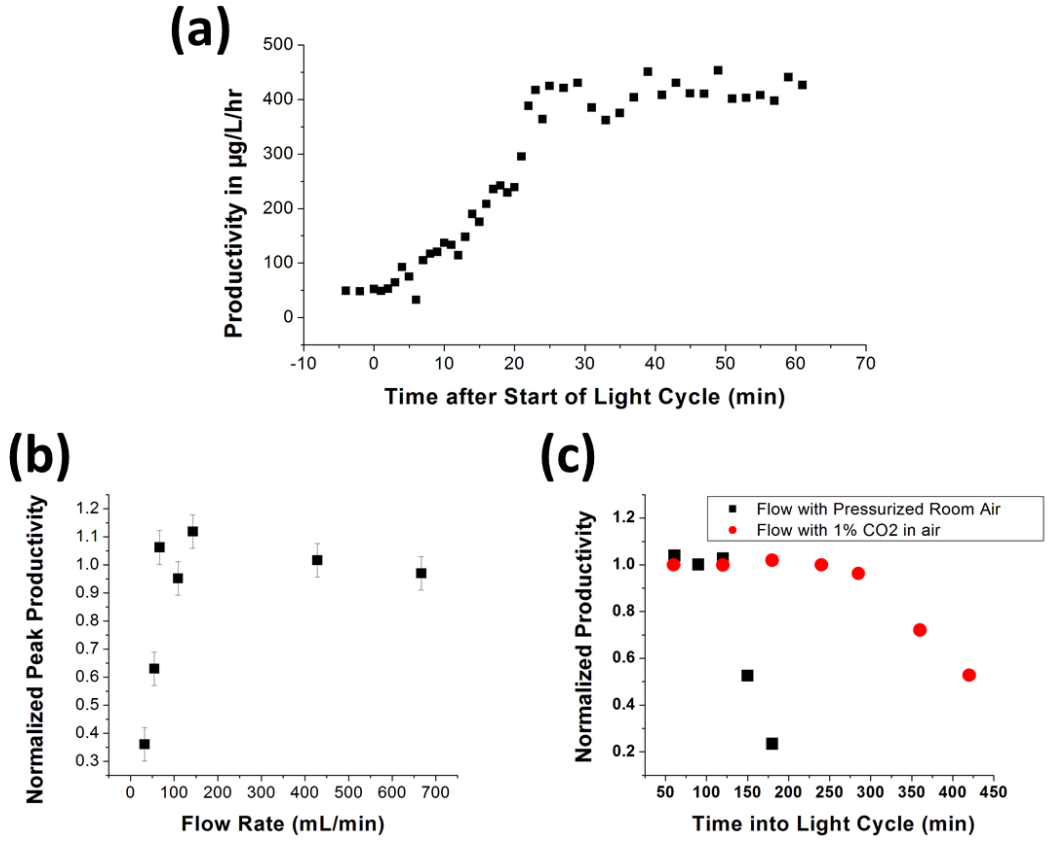

Fig. 4.2: a) Transient Behavior at Beginning of Light Cycle shows that it takes about 25 minutes for reactor to achieve peak productivity, b) Normalized Productivity to Flow Rate reveals a plateauing of productivity past 66mL/min, c) Normalized Productivity over course of Light Cycle for different gas streams

4.4.1 – Measurement Details

The ethylene concentration was sampled an hour after the start of each light cycle. To calculate the ethylene production at this point, we simply multiplied the ethylene concentration with the flow rate to determine productivity rates. Once the LED banks

were turned on, it took about 20-25 minutes for the reactor to start producing at peak productivities as is shown in Fig. 4.2.a. This was expected as it would take some time for the cells in the algae to start producing ethylene which is consistent with what was observed in flat-plate reactors (not reported). The beginning of the run starting from half an hour onwards for several hours corresponded to the peak productivity rates. This seems reasonable because prior to the start of each run, the algae was centrifuged and re-suspended in fresh carbonated media. As the run continued (generally lasting for several hours), we hypothesized that the oxygen build-up and the carbon depletion would result in lower productivities.

This was confirmed in actively aerated gas stream runs shown in Fig. 4.2.c run at relatively high light intensity conditions of 100 µEinsteins $m^{-2}s^{-1}$. As shown in Fig. 4.2.c, there was significant difference between the two gas streams investigated for life cycle productivities. Both gas streams were studied when reactor productivity was close to 400 µg/L/hr at flow rates of 200 +- 100mL/min. Under gas streams consisting of pressurized room air, the PBRs performed at peak productivity for 2 hours. Afterwards, we observed the PBR productivity decrease sharply over an hour to around 20% peak productivity at 3 hours. In contrast, when the PBRs were fed a gas stream of 1% CO2 in air, their ethylene productivities remained constant for almost the entire duration of the light cycle except for the last hour where it decreased to ~55% of peak productivity. Even though the actively aerated gas stream should alleviate oxygen build-up, it probably also removes the carbon source resulting in depleted productivities in the later hours of the light cycle. For the average 7 hour

light cycle used in our experimental runs to grow the algae, this would correspond to an average productivity of 43% that of the peak productivity if we assumed a minimum productivity of 20%. In contrast, the gas stream with 1% CO2 should not only alleviate the oxygen build-up but also resupply the carbon dioxide into the media. As a result, the average productivity over the light cycle corresponds to over 90% the peak productivity measured after an hour. We believe that the decrease in productivities past the 6^{th} hour is probably due to wear and damage to the photosynthetic machinery of the individual cells from usage due to relatively high light intensity conditions even when the bottlenecks associated with carbon limitation and oxygen build-up are alleviated.

4.4.2 Flow rate Optimization

We measured productivities of the photobioreactor as compared to different flow rates during the first two hours of the life cycle run (after waiting half an hour for the flow rate effects to equilibrate). Our results as plotted in Fig. 4.2.b indicated that increasing flow rates beyond a 66mL/min made little difference to improve ethylene collection into the fiber membranes from the reactor culture. The optimal flow rate should in principle optimize the energy output versus the energy required for the gas flow. Previous experiments [111] have determined the operating pressure to be roughly 2 mPsi, and assuming a flow rate of 66mL/min, we realize that the energy required for gas exchange is close to 14mW for our reactors of 15mL which scales to ~1mW/L for mixing. This is an order of magnitude lower in terms of energy required

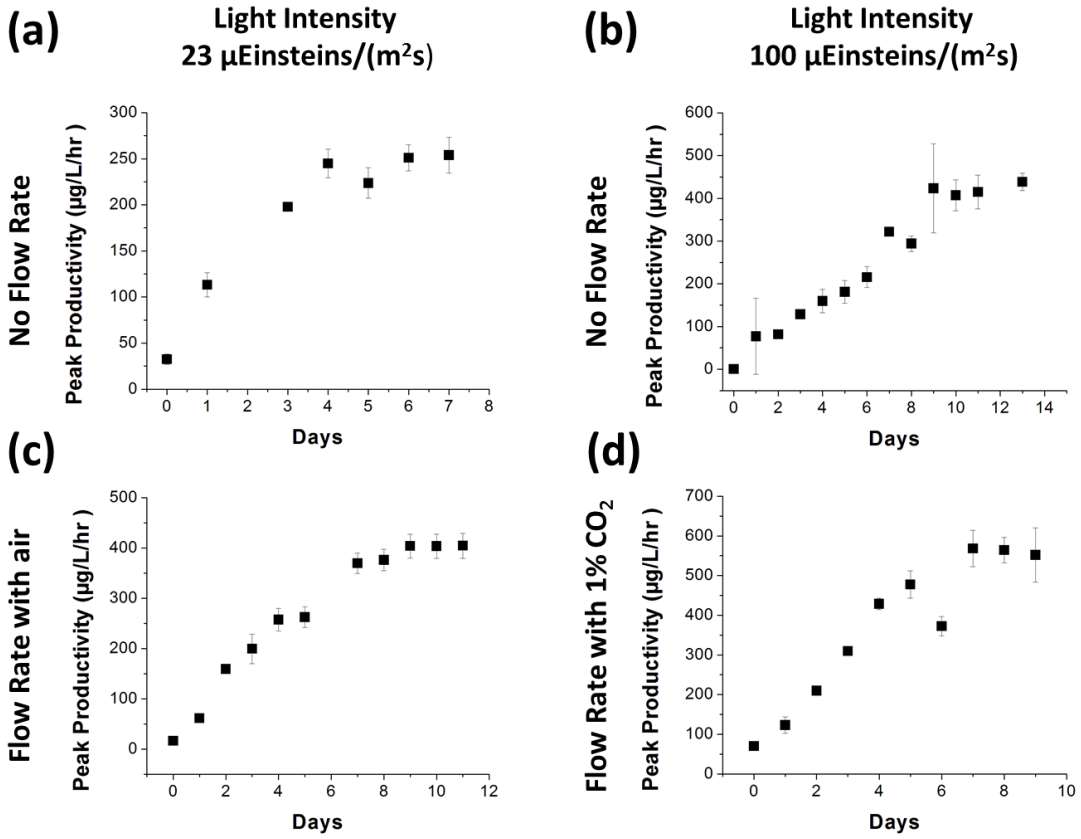

Fig. 4.3: Growth experiments that monitored ethylene productivity performed at (a) low light intensity and passive aeration; (b) high light intensity and passive aeration; (c) low light intensity and active aeration with air; (d) high light intensity with active aeration with 1% CO_2 in air.

for mixing in most PBR systems where even simple systems use ~3W m^{-2} [97] at significantly lower culture densities and production.

4.4.3 System Performance under different gas streams

As shown in Fig. 4.3, the different gas streams were investigated in experimental runs at low and high light intensity conditions to observe productivity growth in the *Synechocystis* cultures. Because of the tightly-packed nature of the reactors, we could not directly get a measure of the cyano-bacteria count through a simple OD_{730} measurement. Rather, the ethylene production was monitored to extrapolate for growth. Generally, the productivity of the culture should depend on the OD of the culture as well as the healthiness of the culture so that the steady-state productivity should correspond directly to the culture density of the system at the time.

At 23 μ Einsteins $m^{-2}s^{-1}$, we were able to observe growth of the cultures under passive room air aeration from close to nominal ethylene production to about 245 μg/L/hr while under actively aerated room air, this production rose to 405 μg/L/hr representing a 65% improvement. We suspect this increase was due to the ability of the aerated gas stream to remove toxic oxygen build-up; it is also possible that the system was carbon-limited even at such low light-intensities starting with daily suspension of 20mM $NaHCO_2$ as the pH of the culture went well beyond pH 9.5. Even so, the addition of carbonated air (not shown here) did not make a significant difference in the steady-state production rates for ethylene. The peak ethylene production efficiency for the aerated runs at these low intensities was markedly higher than that in the SW PBR by close to 35% with ethylene production efficiencies in excess of close to 0.16% calculated in terms of lower heating value of the ethylene produced.

At 100 µ Einsteins $m^{-2}s^{-1}$, we investigated a passive aeration gas stream and an actively aerated 1% CO2 gas stream. The PBR under passive aeration grew from nominal ethylene production values to 420 µg/L/hr although the ramp rate did not vary significantly from either of the runs at 23 µ Einsteins $m^{-2}s^{-1}$ all of which were close to ~45 µg/L/hr/day for the first half of the run. In comparison, under an actively aerated gas stream with 1% CO2, the ethylene production rose to 560 µg/L/hr with much faster ramp rates of ~90 µg/L/hr/day. This corresponded to an improvement in plateau peak productivities of close to 33%. While this is quite significant of an improvement, it is smaller than the improvements seen at lower light intensities by a factor of two. We believe that this is the case because while active aeration is able to alleviate oxygen build-up in the system, it is able to do little about the damage to the photosynthetic machinery by the higher flux of photons which may be a more significant factor.

4.4.4 Optimal PBR Productivities at different OD and Light Intensities

While the carrying capacities corresponded to culture densities that could not be directly measured, we were able to inoculate the reactors at known OD_{730} cultures grown and kept in the exponential phase in flasks. The reactors were then operated under 2 light-dark cycles of 2 hours each that particular day to acclimatize the culture to the reactor after which light-dark cycles of an hour ensued to measure productivities at different light intensities. After two days of use, the culture was

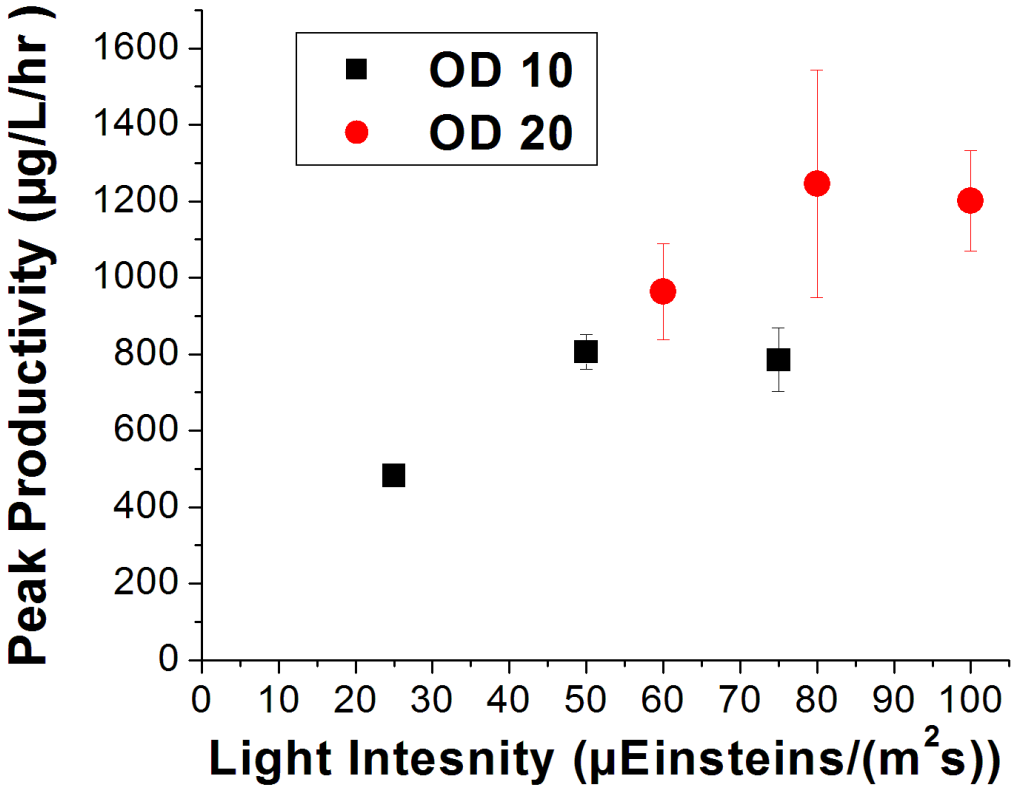

Fig. 4.4: Peak Productivity of HFM reactor with carbonated gas stream input at different intensities loaded with high OD cultures.

retired and new inoculum was used. This was to ensure that there was no significant difference on the OD_{730} caused because of growth in the culture. Ethylene productivities measured in these hollow fiber membrane PBRs run with 1% CO_2 in air outperformed their SWPBR counterparts [108] even when accounting for average productivities as opposed to peak productivities.

As shown in Fig.4.4, at OD 10, we measured peak productivities in excess of 800 µg/L/hr at 50 µ Einsteins $m^{-2}s^{-1}$ as compared to 660 µg/L/hr for the SWPBR

amounting to a 21% improvement at OD 10. While the general production to intensity relationship of the two reactors was roughly the same, the HFM reactor counterpart seems to augment productivities across the entire range of intensities. The same general characteristic held for experiments performed with OD 20 inoculum. The productivities were in excess of 1200 µg/L/hr at both 80 and 100 µ Einsteins $m^{-2}s^{-1}$ yielding a 28% increase in maximum productivities over the SWPBRs.

4.5 Conclusions and Perspectives

In this work, we built and tested an integrated hollow fiber membrane stacked waveguide photobioreactor. We used a genetically modified cyanobacteria *Synechocystis* sp. PCC 6803 strain capable of producing ethylene. We were able to realize that system productivity plateaued with flow rates in excess of 66mL/min which corresponded to a pressure of 2 psi. With our 15mL reactor space, this corresponds to a "gas-mixing" input energy of close to ~1W/L. In addition, at relatively high light intensities of 100 µ Einsteins $m^{-2}s^{-1}$, we were able to show average to peak productivities of close to 90% for an aerated gas stream with 1% CO_2. Growth experiments at lower light intensities of 23 µEinsteins $m^{-2}s^{-1}$ and higher light intensities of 100µEinsteins $m^{-2}s^{-1}$ yielded 65% and 33% improvement in plateau productivities respectively. In addition, we showed a two-fold increase in growth ramp rates with carbonated gas streams, and close to 20% output improvement across light intensities in reactors loaded with high density cultures. We believe that while such an integrated hollow fiber membrane stacked waveguide

photobioreactor is a promising system, further work needs to be done on upscaling and cost modeling for the technology to become competitive.

CHAPTER 5

STACKED WAVEGUIDE REACTORS WITH GRADIENT EMBEDDED SCATTERERS FOR HIGH-CAPACITY WATER CLEANING

5.1 Abstract

In this work, we present a compact water cleaning reactor with stacked layers of waveguides with gradient scatterers to uniformly distribute light to enable augmented water cleaning rates. While there has been a lot of work performed on photocatalytic water cleaning, there have been relatively few pilot plants with high capacity performance. Previous photocatalytic reactors using immersion, external, or distributive lamps suffer from poor light distribution. Here, we use an external UV source to direct photons into stacked waveguide reactors where we scatter the photons uniformly over the length of the waveguide to thin films of TiO_2 catalysts to degrade Methylene Blue. At 10mL/min capacity, we degrade 67% of the organic dye and are able to show a 4.5-5 times improvement over a uniform scatterer design found in most reactors. Finally, we perform some flow rate experiments to characterize the degradation rate constant.

5.2 Introduction

Global population increase and rapid industrialization have put severe strain on clean water resources [18, 112]. It is estimated that around 4 billion people worldwide have limited access to clean water and millions of people die of waterborne diseases annually [113]. The most common methods to treat water involve using physical, chemical or biological processes that nonetheless do not destroy many of the pollutants in the water, mainly highly complex organic compounds chief amongst them halogenated organics[114]. Amongst these organics produced by industrial and agricultural usage are dyes, surfactants, pesticides, and herbicides[18]. In view of worsening trends, it is imperative to develop cheap and efficient methods to treat waste water.

There are currently several technologies used to obtain high-purity water. Phase-transition treatments such as adsorption or coagulation merely transfer the pollutants from one phase to another creating the problem of ultimately disposing of the material [115]. Other methods like sedimentation, filtration and membrane technologies can create secondary pollutants and have high operating costs [116]. Air and stream stripping removes the contaminants into the gas phase creating gas pollution[117] while a proven method like adsorption by activated carbon produces a hazardous solid that must be removed[118]. Biological processes may also be ineffective because of the presence of compounds disabling microbe activity[119]. Chlorination, the most commonly used treatment process, generates carcinogenic byproducts [120, 121]. Generally, the most effective processes are based on the use

of hydroxyl radical compounds like peroxides and ozone; however, these processes use high-energy UV light coupled with the strong oxidants generally of high toxicity[122]. Indeed, some of these processes are destructive in nature and suffer from very low efficiencies which lead to high treatment costs if complete mineralization is required. All of these short-comings in conventional technologies have led to the development of the field of advanced oxidation processes [123]. AO processes create in-situ transitory species which are capable of mineralizing the compounds of interest [124]. One particularly promising technology in this area is heterogeneous photocatalysis which use semiconductor materials like TiO2 and low energy UV photons to achieve the degradation of organic compounds and the deactivation of harmful microbes [113]. The appeal of this technology besides the low costs is its ability to completely mineralize the pollutants into harmless compounds; organic compounds are degraded to carbon dioxide while others are reduced to harmless anions like nitrates, sulfates and chlorides[125]. Practically any pollutant including aliphatics, aromatics, dyes, surfactants, pesticides, and herbicides have been demonstrated in previous literature to be completely mineralized[126].

Although photocatalysis is a very promising technology, there are relatively few pilot-scales plants that are currently in operation [127]. While TiO2 can be activated by sunlight, the intensity of peak solar illumination is too low to enable high capacity for water treatment for a lot of applications without using a lot of land area[128]. On the other hand, the use of external UV lights needs to justify the extra

cost by enabling higher water treatment capacity to still be competitive [129]. Amongst existing reactors are slurry-type reactors where the TiO2 catalysts are suspended in solution [130]. These reactors suffer from poor light illumination and require down-stream collection of the TiO2 particles [127, 130]. On the other hand, fixed bed reactors, using immersion-type, external-type and distributive-type lamps, generally a variation of the annular type reactors suffer from low surface area to volume ratio [131-133]. Innovative-type reactor designs for large-scale applications have also been proposed. Multiple Tube Reactors (MTR) and Tube Light Reactors (TLR) reactors both use waveguides to deliver the UV photons deep into the reactor depth where they are gradually released[132, 134]. Apart from imparting more than 400 times improvement over the classical annular reactors, these designs also have the possibility of being scaled for high-capacity water-treatment applications[132].

One limit of such reactors however is the uneven distribution of light delivered throughout the reactor space[135]. Because these reactor models both rely on waveguides, there is a decay of the internally transmitting light resulting in non-uniform release of the light[135]. One possible solution is to employ waveguides with engineered scatterers that are spatially distributed precisely to scatter the light uniformly within the reactor space. We have utilized such waveguide designs in the past for use in algal photobioreactors[63]. Employing single-waveguide reactors, we were able to demonstrate uniform scattering illumination across the length of the waveguide when integrated over the entire range of scattering angles in the near-field

regime[63]. Such uniform illumination schemes were shown to be superior to their counterparts chemically etched to have uniform surface roughness in delivering more than 40% improvements in growth rates to algal cultures[63].

In this chapter, we demonstrate a photo-catalytic water-splitting device with multiple stacks of waveguides. The waveguides are fabricated with both uniform and engineered scatterer designs to test the validity of the scatterer design. We use a TiO2 sol-gel on top of each layer of waveguides to degrade methylene blue to test organic degradation for water cleaning. At 10mL/min capacity, we demonstrate close to 67% degradation of the organic dye for the reactors with the engineered scatterer waveguides along with close to 4.5-5 times improvement over the uniform scatterer design. We offer a path for upscaling the reactor for high-capacity use.

5.3 Methods

5.3.1 Fabricating the scatterers

SU-8 pillars were fabricated by spinning a 2.8 micron thick layer of SU-8 2002 (Microchem) on 1 mm borosilicate glass slides and patterned through the use of hard contact exposure on the Suss MA6-BA6 Contact Aligner. As shown in Fig. 5.1.c, each SU-8 pillar was 5 μm by 5 μm. The scattering scheme involving the uniform density of SU-8 pillars had a coverage density of 25%, i.e. each pillar was separated from the other on a square lattice by 5 μm. Gradient densities of SU-8 pillars were achieved by

varying the distance from each SU-8 pillar along the length of the waveguide. The chemically etched waveguides were fabricated by applying Armour Etch to glass slides for seven hours followed by rigorous rinsing in water. This etching cream isotropically etched the glass to create a uniform characteristic surface roughness.

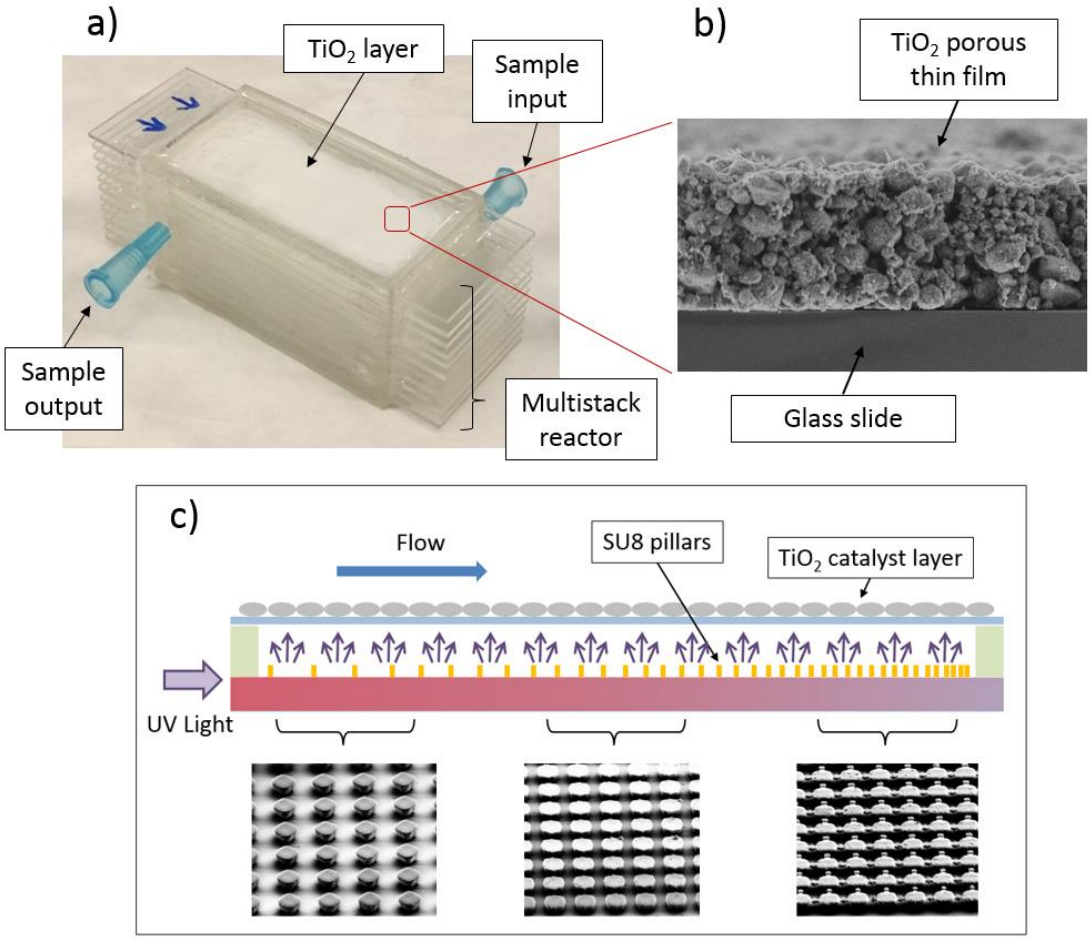

Fig. 5.1: (a) Picture of the stacked waveguide reactor; (b) SEM of the thin-film of TiO_2 catalyst on a cover-slip slide; (c) Schematic of the waveguide with the gradient scatterers enabling uniform illumination.

5.3.2 TiO2 sol-gel

To create the TiO2 sol-gel, we added 0.23 mL of acetylacetone to 70 mL of water and vigorously mixed the solution. 7 g of anatase TiO_2 nanopowder (50 nm from Sigma Aldrich) was mixed in slowly to disperse the powder over the solution. 0.2 mL of a

Triton X-100 was then added to facilitate the spreading of the colloid on the coverslips after which 1.4 g of polyethylene glycol was added into the mixture. The solution was then left to mix for several days before it was ready to use.

5.3.3 Fabricating the waveguides

50 µL of the TiO2 sol-gel were applied to 80 µm coverslips. As shown in Fig. 5.1.b, the sol-gel was distributed evenly over the cover slides to create a uniform thin film. The coverslips were then dried for 2 hours at 80 C after which they were calcinated at 550C for 6 hours in a controlled atmosphere furnace in atmospheric air to treat the catalyst film. The microcover slips with the TiO2 coating were then affixed to the 1mm glass slides and sealed in place with PDMS to create air cladding at the interface to better scatter the light.

5.3.4 Reactor Fabrication and runs

The reactor frames were printed using a 3D printer with a photocurable resin (VeroClear, Objet Geometries Inc.). The dimension on the frame was 7.5 cm x 2.5 cm x 3 cm (length x width x height). As shown in Fig. 5.1.a, the reactor frames consisted of 10 parallel slots reactor separated by 2mm along the height of the reactor for each waveguide. Each layer slot had an influent port for input media and an effluent port for output media on the other side. After the waveguide scatterers were inserted in

each layer, polydimethylsiloxane (PDMS) (Dow Chemicals, Midland, Michigan, USA) was used to affix the waveguides to each layer of the reactor. In all of our experimental runs, we used a 100W Hg lamp as the UV source. Our reactors utilized Methylene Blue as the test organic dye. The percentage degradation of the dye was monitored by analyzing its absorbance at 670 nm.

5.4 Results and Discussion

The light was illuminated into the waveguide through the side where it was totally internally transmitted until it was released either by the presence of a rough surface or by striking a SU-8 pillar with a higher index of refraction (NA = 1.59) than the glass itself. According to Fresnel equations, when light strikes an interface from a medium of lower to higher refractive index, part of the light is transmitted and reflected. As long as the coupling coefficient between the pillars and the waveguide is small, we can expect that both the intensity of the internally reflected wave and scattered wave will decrease exponentially for the case of a constant density of SU-8 pillars along the transmitting direction of the waveguide.

As demonstrated in a previous work [63], if the extinction coefficient is known for the related to the internally transmitted and scattered intensities, one can then precisely distribute the scatterers along a gradient distribution to ensure uniform intensity of scattering along the length of the waveguide as:-

$$SC(x) = {k_i}/{sc_i * (1/k_0 - x)} \quad (5.1)$$

where *sc(x)* is the surface coverage of the scatterers, k_i is the extinction coefficient for a sample with associated surface coverage sc_i and k_0 is given by the following equation:

$$k_0 = {k_{\max}}/{(1 + L * k_{\max})} \quad (5.2)$$

where L is the length of the waveguide and k_{max} is the extinction coefficient as the end of the waveguide which is also the maximum extinction coefficient associated with the maximum surface coverage which is 50% for the case of our pillar SU-8 scatterers.

Of course, the relevant scattered intensities that are relevant need to account for scattering profile over all the scattering angles. To do this, we used shallow channel dyes as reported in previous works (not shown here). The scattered light was used to excite fluorescent dyes in a channel depth of 300 μm within the surface of the waveguides. Images taken over the length of the waveguide allowed for the determination of the relevant extinction coefficient for equation (1). This modeled the 2 μm photocatalyst layer suspended ~120 μm above the waveguide reasonably well.

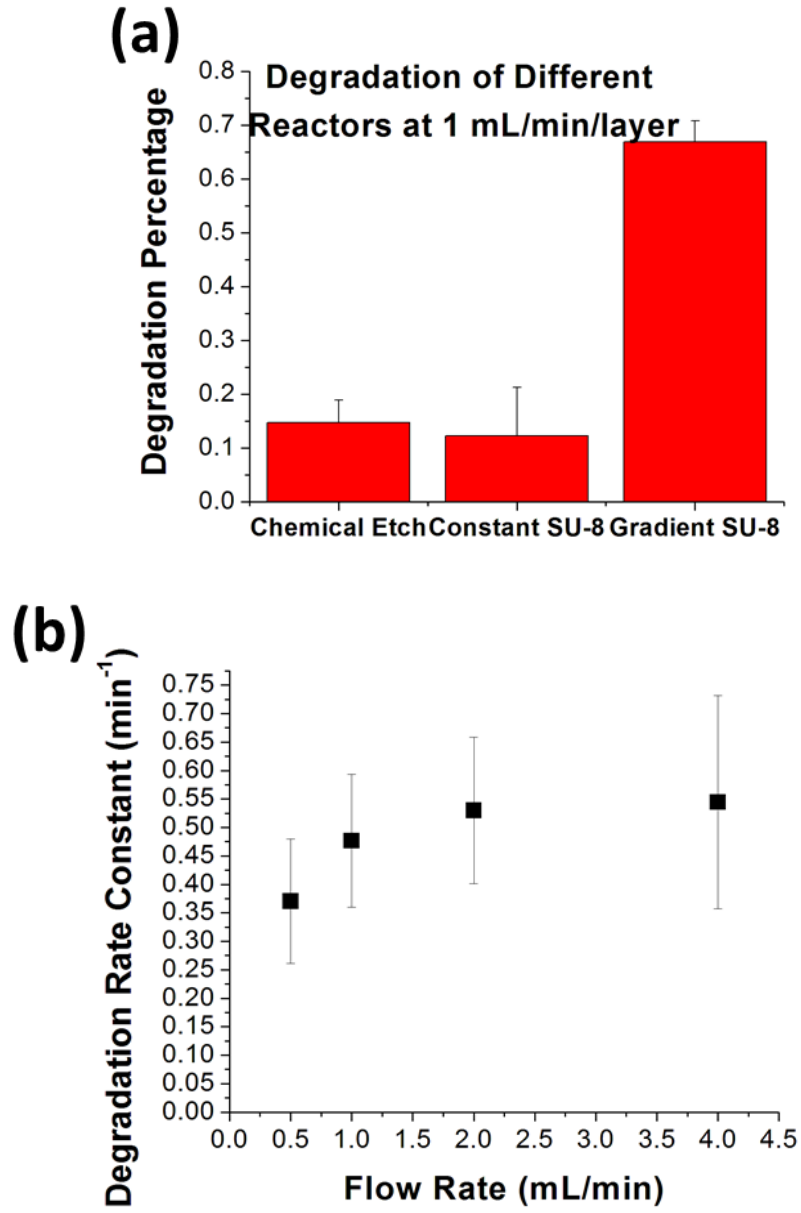

Fig. 5.2: (a) Degradation Percentages of reactors with different scattering schemes for light delivery through the waveguides at capacity of 10mL/min or 1mL/min/layer. (b) Degradation Rate Constant with respect to the different flow rates.

Borosilicate glass is highly absorbing of higher energy UV photons with

wavelengths shorter than 350 nm while SU-8 is highly absorbing for wavelengths shorter than 360 nm. Because the anatase phase of TiO2 is only activated by UV photons smaller than 380 nm, this meant that the wavelength of activation corresponded to 365 nm, the only peak in between 360 nm and 380 nm on the Hg lamp spectrum. Because it was difficult to obtain the necessary filters, the shallow channel dye experiments were performed at higher wavelengths of 630 nm (previously reported) and we assumed there was little difference in the scattering coefficients due to little change in the indices of the relevant media at these two different wavelengths.

Degradation experiments were performed using $3*10^{-5}$ μM Methylene Blue in 1x PBS buffer to keep the media around neutral pH. The activity was calculated by multiplying the flow rates by the percentage of the dye that gets degraded. At 1mL/min going through each layer (10mL/min for entire reactor), the photocatalytic water-cleaning reactor based on the chemical etch scatterers, constant SU-8 scatterers and gradient SU-8 scatterers yielded 15%, 12% and 67% degradation percentages respectively. As shown in Fig. 5.2.a, this yielded a 4.5-5 times improvement in degradation activity for the reactor with the gradient scatterers over the uniform scatterers. We suggest this improvement of the gradient scatterers is because of its more uniform illumination. The uniform scatterer schemes including both the chemical etch and constant SU-8 scatterer scheme exponentially decay in illumination intensity; the front of the waveguides have much more than optimal intensity leading

to photo-saturation, while the back of the waveguides are illuminated with less than optimal intensities leading to sub-optimal degradation rates.

Another salient advantage of our system is also the augmentation of mass transport. Similar optofluidic planar reactors for water cleaning [32] in the past have showed tremendous improvements albeit they were much thinner than the slot channels in our reactor (100μm vs 1mm). The augmentation of mass transport is reported in previous experiments [43] as well and is explained through the following equation:

$$\frac{1}{c} = \frac{1}{C*\Gamma} + \frac{1}{c_m \alpha_v} \tag{5.3}$$

where c is the reaction rate, C is the intrinsic maximum reaction rate, Γ is the Langmuir adsorption coefficient, c_m is the mass diffusivity, and α_v is the surface to volume ratio. $C*\Gamma$ is a function of the chemical properties of the materials, while $c_m*\alpha_v$ is a function of the reactor. Optofluidic reactors have features that enable significantly higher surface to volume ratios over those of conventional reactors, 10,000–30,000 $m^2\ m^{-3}$ in conventional reactors to 600 $m^2\ m^{-3}$ in optofluidic reactors [136]. Indeed, the catalyst film can be characterized as porous which enables high surface to volume ratio. In addition, it is proven that mass diffusivity is generally also higher because the reduced dimensions allow for larger concentration gradients at even moderate flow rates as has been previously demonstrated.

To test the reaction rates, we performed degradation reactions at different flow rates from 0.5mL/min to 4mL/min over one layer. To calculate the degradation reaction, we used to following equation:

$$c = -\log(1-x)/t \qquad (5.4)$$

where c is the degradation constant, x is the degradation percentage, and t is the average retention time of the dye inside the reactor. The degradation constant, c, is plotted in Fig. 5.2.b. As can be seen, it varies from 0.37 to 0.54 min^{-1}. This is an order smaller than optofluidic reactors with smaller dimensions of 100 μm reported previously which found the reaction rate constant to vary from 1.6 to 2.2 min^{-1} but it is significantly larger than the bulk value of 0.015 min^{-1} [32]. This makes sense because while our channel height (1mm) is larger than 100 μm, it should still benefit from improved mass transfer from bulk reactor conditions.

To achieve higher capacity photocatalytic water cleaning reactors will require upscaling the dimensions of the reactor to make the treatment costs more competitive. The gradient distribution for the SU-8 scatterers can be generalized and employed for longer sizes of waveguides. To keep the improvements in mass transport, we suggest that the distance between the waveguides is kept as small as possible. In addition, while the SU-8 scatterer fabrication that we used on our waveguides is very expensive, there are cheaper fabrication methods possible such as hot embossing and

molding. Finally, the use of UV LEDs could provide the cheap source of low-energy UV photons required to activate the reactor.

5.5 Conclusions and Perspectives

In this work, we demonstrate a novel photocatalytic reactor for water cleaning with augmented mass transfer and optical transfer characteristics for high-capacity applications. We use a TiO_2 sol-gel to create a porous thin film of catalyst and stack the layers closely to improve mass transport. In addition, we use SU-8 pillars as scatterers distributed across the waveguide in a gradient to enable uniform illumination across the length of the waveguide. We achieve 67% degradation of the Methylene Blue dye at 10mL/min capacity and show a 4.5-5 times improvement over typical waveguide light delivery configurations. The degradation rate constant is characterized in flow rate experiments and shown to be between $0.37 – 0.54\ min^{-1}$.

CHAPTER 6

CONCLUSIONS AND DISCUSSIONS

In the first part of the thesis, we have used for the first time, to our knowledge, a micro-fluidic platform to study photocatalytic water-splitting. We demonstrate how carrying out the reaction in an optofluidic environment significantly reduces the material costs and time associated with carrying out redox-mediated water-splitting reactions. We have used this platform to study the reaction kinetics of Pt-TiO_2 which we found agreed with previous literature. Additionally, we demonstrated that such platforms have the potential to enhance the reaction rates and efficiencies by improving mass transport. To this effect, we showed that simply increasing the flow rates yielded at least ~2-fold improvements in reaction rates. We suggest that such an optofluidic platform could be used to rapidly and cheaply perform kinetic studies on different photocatalysts to screen for potential catalysts and optimize their reaction conditions.

In the second part, we designed and fabricated light scattering waveguides that uniformly illuminated photo-bioreactors to improve growth of algal cultures. This gradient scattering scheme was tested along with other scattering schemes and was shown to be superior both in terms of the uniformity of growth and total coverage resulting in improvements of growth rates of 40%. Our reactors can be easily stacked to enable us to distribute light efficiently when stacked in close proximity and are

compatible with genetically modified strains that could produce biofuels directly. Ultimately, we hope this will allow for the upscaling of existing stacked waveguide photobioreactors enabling pilot scale studies to better determine costs associated with these platforms for algal cultivation.

Third, we built and tested an integrated hollow fiber membrane stacked waveguide photobioreactor. We used a genetically modified cyanobacteria *Synechocystis* sp. PCC 6803 strain capable of producing ethylene. We were able to realize that system productivity plateaued with flow rates in excess of a certain amount corresponding to a "gas-mixing" input energy of close to ~1W/L. In addition, at relatively high light intensities, we were able to show average to peak productivities of close to 90% for an aerated gas stream with 1% CO_2. Growth experiments at lower light intensities and higher light intensities yielded 65% and 33% improvement in plateau productivities respectively. In addition, we showed a two-fold increase in growth ramp rates with carbonated gas streams, and close to 20% output improvement across light intensities in reactors loaded with high density cultures. We believe that while such an integrated hollow fiber membrane stacked waveguide photobioreactor is a promising system, further work needs to be done on upscaling and cost modeling for the technology to become competitive.

Finally, we demonstrate a novel photocatalytic reactor for water cleaning with augmented mass transfer and optical transfer characteristics for high-capacity applications. We use a TiO_2 sol-gel to create a porous thin film of catalyst and stack the layers closely to improve mass transport. In addition, we use previous gradient

scattering schemes to enable uniform light delivery. We achieve 67% degradation of a test organic compound at 10mL/min capacity and show a 4.5-5 times improvement over typical waveguide light delivery configurations. The degradation rate constant is characterized in flow rate experiments and shown to be consistent with previous data. Further optimization of the system is possible by further miniaturization. In addition, future work needs to evaluate the economic costs of such a reactor model to test for commercial viability.

BIBLIOGRAPHY

1. Administration", U.E.I., *Monthly Energy Review*, D.o. Energy, Editor. 2012: Washington DC.

2. Dong, L., et al., *Adaptive liquid microlenses activated by stimuli-responsive hydrogels.* Nature, 2006. **442**(7102): p. 551-554.

3. Kim, H., et al., *Structural colour printing using a magnetically tunable and lithographically fixable photonic crystal.* Nature Photonics, 2009. **3**(9): p. 534-540.

4. Ohko, Y., A. Fujishima, and K. Hashimoto, *Kinetic analysis of the photocatalytic degradation of gas-phase 2-propanol under mass transport-limited conditions with a TiO(2) film photocatalyst.* Journal of Physical Chemistry B, 1998. **102**(10): p. 1724-1729.

5. Erickson, D., D. Sinton, and D. Psaltis, *Optofluidics for energy applications.* Nature Photonics, 2011. **5**(10): p. 583-590.

6. Chiou, P.Y., A.T. Ohta, and M.C. Wu, *Massively parallel manipulation of single cells and microparticles using optical images.* Nature, 2005. **436**(7049): p. 370-372.

7. Mandal, S., J.M. Goddard, and D. Erickson, *A multiplexed optofluidic biomolecular sensor for low mass detection.* Lab on a Chip, 2009. **9**(20): p. 2924-2932.

8. Administration, E.I., *Annual Energy Outlook*, U.D.o. Energy, Editor. 2005: Washington, DC.

9. Holdren, J.P., *The Energy Innovation Imperative: Addressing Oil Dependence, Climate Change, and Other 21st Century Energy Challenges.* Innovations: Technology, Governance, Globalization, 2006. **1**(2): p. 3-23.

10. Change, I.P.o.C., *Climate Change 2001, Synthesis Report Summary for Policymakers*, I.P.o.C. Change, Editor. 2001, Third Assessment Report: Washington, DC.

11. Wigley, T.M.L., R. Richels, and J.A. Edmonds, *Economic and environmental choices in the stabilization of atmospheric CO2 concentrations.* Nature, 1996. **379**(6562): p. 240-243.

12. Deutch, J., et al., *The future of nuclear power.* an MIT Interdisciplinary Study, http://web. mit. edu/nuclearpower, 2003.

13. Metz, B., et al., *Carbon dioxide capture and storage.* 2005.

14. Goldemberg, J., *World Energy Assessment: Energy and the challenge of sustainability*. 2000: United Nations Pubns.

15. Lewis, N.S. and D.G. Nocera, *Powering the planet: Chemical challenges in solar energy utilization.* Proceedings of the National Academy of Sciences, 2006. **103**(43): p. 15729-15735.

16. Lewis, N.S. and D.G. Nocera, *Powering the planet: Chemical challenges in solar energy utilization.* Proceedings of the National Academy of Sciences of the United States of America, 2007. **104**(50): p. 20142-20142.

17. Richardson, S.D., *Environmental Mass Spectrometry: Emerging Contaminants and Current Issues.* Analytical Chemistry, 2012. **84**(2): p. 747-778.

18. Wintgens, T., et al., *Emerging contaminants and treatment options in water recycling for indirect potable use.* Water Science and Technology, 2008. **57**(1): p. 99-107.

19. Ahmed, T., et al., *Emerging nanotechnology-based methods for water purification: a review.* Desalination and Water Treatment, 2014. **52**(22-24): p. 4089-4101.

20. Manz, A., N. Graber, and H.M. Widmer, *Miniaturized Total Chemical-Analysis Systems - a Novel Concept for Chemical Sensing*. Sensors and Actuators B-Chemical, 1990. **1**(1-6): p. 244-248.

21. Pawlak, M., et al., *Zeptosens' protein microarrays: A novel high performance microarray platform for low abundance protein analysis.* Proteomics, 2002. **2**(4): p. 383-393.

22. Lee, H.J., T.T. Goodrich, and R.M. Corn, *SPR imaging measurements of 1-D and 2-D DNA microarrays created from microfluidic channels on gold thin films.* Analytical Chemistry, 2001. **73**(22): p. 5525-5531.

23. Psaltis, D., S.R. Quake, and C.H. Yang, *Developing optofluidic technology through the fusion of microfluidics and optics.* Nature, 2006. **442**(7101): p. 381-386.

24. Monat, C., P. Domachuk, and B.J. Eggleton, *Integrated optofluidics: A new river of light.* Nature Photonics, 2007. **1**(2): p. 106-114.

25. Erickson, D., et al., *Nanofluidic tuning of photonic crystal circuits.* Optics Letters, 2006. **31**(1): p. 59-61.

26. Karnutsch, C., et al., *Temperature stabilization of optofluidic photonic crystal cavities.* Applied Physics Letters, 2009. **94**(23).

27. Kuiper, S. and B.H.W. Hendriks, *Variable-focus liquid lens for miniature cameras.* Applied Physics Letters, 2004. **85**(7): p. 1128-1130.

28. Li, Z.Y., et al., *Single mode optofluidic distributed feedback dye laser.* Optics Express, 2006. **14**(2): p. 696-701.

29. Rich, R.L. and D.G. Myszka, *Survey of the year 2006 commercial optical biosensor literature.* Journal of Molecular Recognition, 2007. **20**(5): p. 300-366.

30. Heng, X., et al., *Optofluidic microscopy - a method for implementing a high resolution optical microscope on a chip.* Lab on a Chip, 2006. **6**(10): p. 1274-1276.

31. Yang, A.H.J., et al., *Optical manipulation of nanoparticles and biomolecules in sub-wavelength slot waveguides.* Nature, 2009. **457**(7225): p. 71-75.

32. Lei, L., et al., *Optofluidic planar reactors for photocatalytic water treatment using solar energy*. Biomicrofluidics, 2010. **4**(4).

33. Lee, M.T., et al., *Hydrogen production with a solar steam-methanol reformer and colloid nanocatalyst.* International Journal of Hydrogen Energy, 2010. **35**(1): p. 118-126.

34. Kondo, T., T. Wakayama, and J. Miyake, *Efficient hydrogen production using a multi-layered photobioreactor and a photosynthetic bacterium mutant with reduced pigment.* International Journal of Hydrogen Energy, 2006. **31**(11): p. 1522-1526.

35. Chen, Y.F., et al., *Optofluidic opportunities in global health, food, water and energy*. Nanoscale, 2012. **4**(16): p. 4839-4857.

36. Yager, P., G.J. Domingo, and J. Gerdes, *Point-of-care diagnostics for global health.* Annual Review of Biomedical Engineering, 2008. **10**: p. 107-144.

37. Chin, C.D., et al., *Microfluidics-based diagnostics of infectious diseases in the developing world.* Nature Medicine, 2011. **17**(8): p. 1015-U138.

38. Scott, N.R., *Nanotechnology and animal health.* Revue Scientifique Et Technique-Office International Des Epizooties, 2005. **24**(1): p. 425-432.

39. *Bio-Farms for Nutraceuticals: Functional Food and Safety Control by Biosensors.* Bio-Farms for Nutraceuticals: Functional Food and Safety Control by Biosensors, 2010. **698**: p. 1-334.

40. Llorent-Martinez, E.J., et al., *Trends in flow-based analytical methods applied to pesticide detection: A review.* Analytica Chimica Acta, 2011. **684**(1-2): p. 30-39.

41. Chong, M.N., et al., *Recent developments in photocatalytic water treatment technology: A review.* Water Research, 2010. **44**(10): p. 2997-3027.

42. Chen, T.C. and C.D. Ho, *Immediate assisted solar direct contact membrane distillation in saline water desalination.* Journal of Membrane Science, 2010. **358**(1-2): p. 122-130.

43. Ahsan, S.S., A. Gumus, and D. Erickson, *Redox mediated photocatalytic water-splitting in optofluidic microreactors.* Lab on a Chip, 2013. **13**(3): p. 409-414.

44. Klass, D.L., *Biomass for Renewable Energy, Fuels, and Chemicals*. 1998: Elsevier Science.

45. Morton, O., *Solar energy: A new day dawning?: Silicon Valley sunrise.* Nature, 2006. **443**(7107): p. 19-22.

46. Herrmann, J.M., *Heterogeneous photocatalysis: fundamentals and applications to the removal of various types of aqueous pollutants.* Catalysis Today, 1999. **53**(1): p. 115-129.

47. Mo, J.H., et al., *Photocatalytic purification of volatile organic compounds in indoor air: A literature review.* Atmospheric Environment, 2009. **43**(14): p. 2229-2246.

48. Wei, C., et al., *Bactericidal Activity of Tio2 Photocatalyst in Aqueous-Media - toward a Solar-Assisted Water Disinfection System.* Environmental Science & Technology, 1994. **28**(5): p. 934-938.

49. Fujishima, A. and K. Honda, *Electrochemical Photolysis of Water at a Semiconductor Electrode.* Nature, 1972. **238**(5358): p. 37-+.

50. Kudo, A. and Y. Miseki, *Heterogeneous photocatalyst materials for water splitting.* Chemical Society Reviews, 2009. **38**(1): p. 253-278.

51. Tong, H., et al., *Nano-photocatalytic Materials: Possibilities and Challenges.* Advanced Materials, 2012. **24**(2): p. 229-251.

52. Maeda, K., et al., *Efficient Nonsacrificial Water Splitting through Two-Step Photoexcitation by Visible Light using a Modified Oxynitride as a Hydrogen Evolution Photocatalyst.* Journal of the American Chemical Society, 2010. **132**(16): p. 5858-5868.

53. Shi, J.W., et al., *Immobilization of TiO2 films on activated carbon fiber and their photocatalytic degradation properties for dye compounds with different molecular size.* Catalysis Communications, 2008. **9**(9): p. 1846-1850.

54. Ge, L., et al., *Fabrication and characterization of nano TiO2 thin films at low temperature.* Materials Research Bulletin, 2006. **41**(9): p. 1596-1603.

55. Lu, H., M.A. Schmidt, and K.F. Jensen, *Photochemical reactions and on-line UV detection in microfabricated reactors.* Lab on a Chip, 2001. **1**(1): p. 22-28.

56. Lindstrom, H., R. Wootton, and A. Iles, *High surface area titania photocatalytic microfluidic reactors.* Aiche Journal, 2007. **53**(3): p. 695-702.

57. Gorges, R., S. Meyer, and G. Kreisel, *Photocatalysis in microreactors.* Journal of Photochemistry and Photobiology a-Chemistry, 2004. **167**(2-3): p. 95-99.

58. Wang, N., et al., *Microfluidic photoelectrocatalytic reactors for water purification with an integrated visible-light source.* Lab on a Chip, 2012. **12**(20): p. 3983-3990.

59. Abe, R., et al., *A new type of water splitting system composed of two different TiO2 photocatalysts (anatase, rutile) and a IO3-/I- shuttle redox mediator.* Chemical Physics Letters, 2001. **344**(3-4): p. 339-344.

60. Galinska, A. and J. Walendziewski, *Photocatalytic water splitting over Pt-TiO2 in the presence of sacrificial reagents.* Energy & Fuels, 2005. **19**(3): p. 1143-1147.

61. Mishra, S.P. and N. Srinivasu, *Radiotracer Technique in Adsorption Study .9. Adsorption of Iodide-Ions on Titanium(Iv) Oxide Powder.* Applied Radiation and Isotopes, 1992. **43**(6): p. 789-793.

62. Hachiya, K., et al., *Study of the Adsorption-Desorption of Io-3- on a Tio-2 Surface by Means of Relaxation Techniques.* Journal of Physical Chemistry, 1980. **84**(18): p. 2292-2296.

63. Ahsan, S.S., et al., *Engineered surface scatterers in edge-lit slab waveguides to improve light delivery in algae cultivation.* Optics Express, 2014. **22**(21): p. A1526-A1537.

64. Cox, P.M., et al., *Acceleration of global warming due to carbon-cycle feedbacks in a coupled climate model.* Nature, 2000. **408**(6809): p. 184-7.

65. Lewis, N.S. and D.G. Nocera, *Powering the planet: chemical challenges in solar energy utilization.* Proc Natl Acad Sci U S A, 2006. **103**(43): p. 15729-35.

66. Chisti, Y., *Biodiesel from microalgae.* Biotechnology Advances, 2007. **25**(3): p. 294-306.

67. Pimentel, D. and T.W. Patzek, *Ethanol production using corn, switchgrass, and wood; biodiesel production using soybean and sunflower.* Natural resources research, 2005. **14**(1): p. 65-76.

68. Lam, M.K. and K.T. Lee, *Microalgae biofuels: A critical review of issues, problems and the way forward.* Biotechnology Advances, 2012. **30**(3): p. 673-90.

69. Chen, C.Y., et al., *Cultivation, photobioreactor design and harvesting of microalgae for biodiesel production: a critical review.* Bioresour Technol, 2011. **102**(1): p. 71-81.

70. Beal, C.M., et al., *The Energy Return on Investment for Algal Biocrude: Results for a Research Production Facility.* Bioenergy Research, 2012. **5**(2): p. 341-362.

71. Wijffels, R.H. and M.J. Barbosa, *An Outlook on Microalgal Biofuels.* Science, 2010. **329**(5993): p. 796-799.

72. Janssen, M., et al., *Enclosed outdoor photobioreactors: Light regime, photosynthetic efficiency, scale-up, and future prospects.* Biotechnology and Bioengineering, 2003. **81**(2): p. 193-210.

73. Grima, E.M., et al., *Photobioreactors: light regime, mass transfer, and scaleup.* Journal of Biotechnology, 1999. **70**(1-3): p. 231-247.

74. Posten, C., *Design principles of photo-bioreactors for cultivation of microalgae.* Engineering in Life Sciences, 2009. **9**(3): p. 165-177.

75. Lehr, F. and C. Posten, *Closed photo-bioreactors as tools for biofuel production.* Current Opinion in Biotechnology, 2009. **20**(3): p. 280-285.

76. Lee, C.-G., *Calculation of light penetration depth in photobioreactors.* Biotechnology and Bioprocess Engineering, 1999. **4**(1): p. 78-81.

77. Bosma, R., et al., *Prediction of volumetric productivity of an outdoor photobioreactor.* Biotechnology and Bioengineering, 2007. **97**(5): p. 1108-1120.

78. Grima, E.M., et al., *A study on simultaneous photolimitation and photoinhibition in dense microalgal cultures taking into account incident and averaged irradiances.* Journal of Biotechnology, 1996. **45**(1): p. 59-69.

79. Ugwu, C.U., H. Aoyagi, and H. Uchiyama, *Photobioreactors for mass cultivation of algae.* Bioresource Technology, 2008. **99**(10): p. 4021-4028.

80. Torkamani, S., et al., *Plasmon-enhanced microalgal growth in miniphotobioreactors.* Applied Physics Letters, 2010. **97**(4).

81. Jung, E.E., et al., *Slab waveguide photobioreactors for microalgae based biofuel production.* Lab on a Chip, 2012. **12**(19): p. 3740-3745.

82. Ooms, M.D., et al., *Evanescent photosynthesis: exciting cyanobacteria in a surface-confined light field.* Physical Chemistry Chemical Physics, 2012. **14**(14): p. 4817-4823.

83. Mori, K., et al., *Design for a bioreactor with sunlight supply and operations systems for use in the space environment.* Adv Space Res, 1989. **9**(8): p. 161-8.

84. Chen, C.Y., et al., *Phototrophic hydrogen production in photobioreactors coupled with solar-energy-excited optical fibers.* International Journal of Hydrogen Energy, 2008. **33**(23): p. 6886-6895.

85. Harbers, G., W. Timmers, and W. Sillevis-Smitt, *LED backlighting for LCD HDTV.* Journal of the Society for Information Displays, 2012. **10**(4): p. 347-350.

86. Chang, J.G. and Y.B. Fang, *Dot-pattern design of a light guide in an edge-lit backlight using a regional partition approach.* Optical Engineering, 2007. **46**(4).

87. Son, C.G., et al., *Improvement of Color and Luminance Uniformity of the Edge-Lit Backlight Using the RGB LEDs.* Journal of the Optical Society of Korea, 2011. **15**(3): p. 272-277.

88. Derlofske, J.F.V., *Computer modeling of LED light pipe systems for uniform display illumination.* SPIE Proceedings, 2001. **4445**: p. 119-129.

89. Ogbonna, J.C., T. Soejima, and H. Tanaka, *An integrated solar and artificial light system for internal illumination of photobioreactors.* Journal of Biotechnology, 1999. **70**(1-3): p. 289-97.

90. Zijffers, J.W.F., et al., *Design process of an area-efficient photobioreactor.* Marine Biotechnology, 2008. **10**(4): p. 404-415.

91. del Campo, A. and C. Greiner, *SU-8: a photoresist for high-aspect-ratio and 3D submicron lithography.* Journal of Micromechanics and Microengineering, 2007. **17**(6): p. R81-R95.

92. Ungerer, J., et al., *Sustained photosynthetic conversion of CO2 to ethylene in recombinant cyanobacterium Synechocystis 6803.* Energy & Environmental Science, 2012. **5**(10): p. 8998-9006.

93. Kalontarov, M., et al., *In situ hollow fiber membrane facilitated CO2 delivery to a cyanobacterium for enhanced productivity.* RSC Adv., 2013.

94. Zhao, Y.J., et al., *Effects of various LED light wavelengths and intensities on microalgae-based simultaneous biogas upgrading and digestate nutrient reduction process.* Bioresource Technology, 2013. **136**: p. 461-468.

95. Chen, C.Y., et al., *Cultivation, photobioreactor design and harvesting of microalgae for biodiesel production: A critical review.* Bioresource Technology, 2011. **102**(1): p. 71-81.

96. Greenwell, H.C., et al., *Placing microalgae on the biofuels priority list: a review of the technological challenges.* Journal of the Royal Society Interface, 2010. **7**(46): p. 703-726.

97. Posten, C. and G. Schaub, *Microalgae and terrestrial biomass as source for fuels-A process view.* Journal of Biotechnology, 2009. **142**(1): p. 64-69.

98. Rodolfi, L., et al., *Microalgae for Oil: Strain Selection, Induction of Lipid Synthesis and Outdoor Mass Cultivation in a Low-Cost Photobioreactor.* Biotechnology and Bioengineering, 2009. **102**(1): p. 100-112.

99. Yun, Y.S., et al., *Carbon dioxide fixation by algal cultivation using wastewater nutrients.* Journal of Chemical Technology and Biotechnology, 1997. **69**(4): p. 451-455.

100. Pires, J.C.M., et al., *Carbon dioxide capture from flue gases using microalgae: Engineering aspects and biorefinery concept.* Renewable & Sustainable Energy Reviews, 2012. **16**(5): p. 3043-3053.

101. Mata, T.M., A.A. Martins, and N.S. Caetano, *Microalgae for biodiesel production and other applications: A review.* Renewable & Sustainable Energy Reviews, 2010. **14**(1): p. 217-232.

102. Wijffels, R.H., M.J. Barbosa, and M.H.M. Eppink, *Microalgae for the production of bulk chemicals and biofuels.* Biofuels Bioproducts & Biorefining-Biofpr, 2010. **4**(3): p. 287-295.

103. Grobbelaar, J.U., *Factors governing algal growth in photobioreactors: the "open" versus "closed" debate.* Journal of Applied Phycology, 2009. **21**(5): p. 489-492.

104. Grobbelaar, J.U., *Microalgal biomass production: challenges and realities.* Photosynthesis Research, 2010. **106**(1-2): p. 135-144.

105. Beal, C.M., et al., *Energy Return on Investment for Algal Biofuel Production Coupled with Wastewater Treatment.* Water Environment Research, 2012. **84**(9): p. 692-710.

106. Norsker, N.H., et al., *Microalgal production - A close look at the economics.* Biotechnology Advances, 2011. **29**(1): p. 24-27.

107. Jung, E.E., et al., *Stacked optical waveguide photobioreactor for high density algal cultures.* Bioresource Technology, 2014. **171**: p. 495-499.

108. Jain, A., et al., *Optimal Intensity and Biomass Density for Biofuel Production in a Thin Light-Path Photobioreactor.* 2015.

109. Kalontarov, M., et al., *In situ hollow fiber membrane facilitated CO2 delivery to a cyanobacterium for enhanced productivity.* Rsc Advances, 2013. **3**(32): p. 13203-13209.

110. Kalontarov, M., et al., *Hollow fibre membrane arrays for CO2 delivery in microalgae photobioreactors.* Rsc Advances, 2014. **4**(3): p. 1460-1468.

111. Federspiel, W.J., J.L. Williams, and B.G. Hattler, *Gas Flow Dynamics in Hollow Fiber Membranes.* AlChE, 1996. **42**(7).

112. Richardson, S.D., *Environmental mass spectrometry: Emerging contaminants and current issues.* Analytical Chemistry, 2008. **80**(12): p. 4373-4402.

113. Malato, S., et al., *Decontamination and disinfection of water by solar photocatalysis: Recent overview and trends.* Catalysis Today, 2009. **147**(1): p. 1-59.

114. Legrini, O., E. Oliveros, and A.M. Braun, *Photochemical Processes for Water-Treatment.* Chemical Reviews, 1993. **93**(2): p. 671-698.

115. Padmanabhan, P.V.A., et al., *Nano-crystalline titanium dioxide formed by reactive plasma synthesis.* Vacuum, 2006. **80**(11-12): p. 1252-1255.

116. Gaya, U.I. and A.H. Abdullah, *Heterogeneous photocatalytic degradation of organic contaminants over titanium dioxide: A review of fundamentals, progress and problems.* Journal of Photochemistry and Photobiology C-Photochemistry Reviews, 2008. **9**(1): p. 1-12.

117. Nirmalakhandan, N., Y.H. Lee, and R.E. Speece, *Designing a Cost-Efficient Air-Stripping Process.* Journal American Water Works Association, 1987. **79**(1): p. 56-63.

118. Stenzel, M.H., *Remove Organics by Activated Carbon Adsorption.* Chemical Engineering Progress, 1993. **89**(4): p. 36-43.

119. Blackburn, J.W., W.L. Troxler, and G.S. Sayler, *Prediction of the fates of organic chemicals in a biological treatment process—an overview.* Environmental Progress, 1984. **3**(3): p. 163-176.

120. Lu, J.F., et al., *Evaluation of disinfection by-products formation during chlorination and chloramination of dissolved natural organic matter fractions isolated from a filtered river water.* Journal of Hazardous Materials, 2009. **162**(1): p. 140-145.

121. Yang, H. and H. Cheng, *Controlling nitrite level in drinking water by chlorination and chloramination.* Separation and Purification Technology, 2007. **56**(3): p. 392-396.

122. Hagfeldt, A. and M. Gratzel, *Light-Induced Redox Reactions in Nanocrystalline Systems.* Chemical Reviews, 1995. **95**(1): p. 49-68.

123. Esplugas, S., et al., *Comparison of different advanced oxidation processes for phenol degradation.* Water Research, 2002. **36**(4): p. 1034-1042.

124. Pera-Titus, M., et al., *Degradation of chlorophenols by means of advanced oxidation processes: a general review.* Applied Catalysis B-Environmental, 2004. **47**(4): p. 219-256.

125. Fox, M.A. and M.T. Dulay, *Heterogeneous Photocatalysis.* Chemical Reviews, 1993. **93**(1): p. 341-357.

126. Matthews, R.W., *Photocatalytic Oxidation of Organic Contaminants in Water - an Aid to Environmental Preservation.* Pure and Applied Chemistry, 1992. **64**(9): p. 1285-1290.

127. Bahnemann, D., *Photocatalytic water treatment: solar energy applications.* Solar Energy, 2004. **77**(5): p. 445-459.

128. Ray, A.K. and A.A.C.M. Beenackers, *Novel swirl-flow reactor for kinetic studies of semiconductor photocatalysis.* Aiche Journal, 1997. **43**(10): p. 2571-2578.

129. Mills, A., R.H. Davies, and D. Worsley, *Water-Purification by Semiconductor Photocatalysis.* Chemical Society Reviews, 1993. **22**(6): p. 417-425.

130. Yurdakal, S., et al., *Photodegradation of pharmaceutical drugs in aqueous TiO2 suspensions: Mechanism and kinetics.* Catalysis Today, 2007. **129**(1-2): p. 9-15.

131. Ray, A.K., *A new photocatalytic reactor for destruction of toxic water pollutants by advanced oxidation process.* Catalysis Today, 1998. **44**(1-4): p. 357-368.

132. Ray, A.K. and A.A.C.M. Beenackers, *Development of a new photocatalytic reactor for water purification.* Catalysis Today, 1998. **40**(1): p. 73-83.

133. Peill, N.J. and M.R. Hoffmann, *Development and Optimization of a Tio2-Coated Fiber Optic Cable Reactor - Photocatalytic Degradation of 4-Chlorophenol.* Abstracts of Papers of the American Chemical Society, 1995. **210**: p. 128-ENVR.

134. Ray, A.K. and A.A.C.M. Beenackers, *Novel photocatalytic reactor for water purification.* Aiche Journal, 1998. **44**(2): p. 477-483.

135. Mukherjee, P.S. and A.K. Ray, *Major challenges in the design of a large-scale photocatalytic reactor for water treatment.* Chemical Engineering & Technology, 1999. **22**(3): p. 253-260.

136. Wang, N., et al., *Microfluidic photoelectrocatalytic reactors for water purification with an integrated visible-light source.* Lab on a Chip, 2012. **12**(20): p. 3983-3990.